

Finding a way through the "misty" evaluation of the flammability and explosivity of kerosene aerosols

Stephanie El-Zahlanieh, Idalba Souza dos Santos, Shyarinya Sivabalan, David Brunello, Benoit Tribouilloy, Alexis Vignes, Olivier Dufaud

▶ **To cite this version:**

Stephanie El-Zahlanieh, Idalba Souza dos Santos, Shyarinya Sivabalan, David Brunello, Benoit Tribouilloy, et al.. Finding a way through the "misty" evaluation of the flammability and explosivity of kerosene aerosols. Fuel, 2022, 328, pp.125275. 10.1016/j.fuel.2022.125275 . ineris-03847279

HAL Id: ineris-03847279
https://ineris.hal.science/ineris-03847279

Submitted on 21 Nov 2022

HAL is a multi-disciplinary open access archive for the deposit and dissemination of scientific research documents, whether they are published or not. The documents may come from teaching and research institutions in France or abroad, or from public or private research centers.

L'archive ouverte pluridisciplinaire **HAL**, est destinée au dépôt et à la diffusion de documents scientifiques de niveau recherche, publiés ou non, émanant des établissements d'enseignement et de recherche français ou étrangers, des laboratoires publics ou privés.

Finding a way through the "misty" evaluation of the flammability and explosivity of kerosene aerosols

Stephanie El-Zahlanieh[a,b], Idalba Souza Dos Santos[a], Shyarinya Sivabalan[a], David Brunello[a], Benoit Tribouilloy[b], Alexis Vignes[b], Olivier Dufaud[a]

[a] LRGP, Université de Lorraine, CNRS, LRGP, F-54000, Nancy, France

[b] INERIS, Fire, Dispersion and Explosion Division, Parc Technologique ALATA Verneuil-en-Halatte, France

olivier.dufaud@univ-lorraine.fr

stephanie.el-zahlanieh@univ-lorraine.fr

Abstract

In the context of assessing hydrocarbon mist ignition sensitivity and explosion severity, an original test method is proposed, focusing on kerosene JetA1 mists but is applicable to other hydrocarbons. Experiments were carried out in a modified apparatus based on the 20L explosion sphere. Fine control of the gas/liquid ratio and flow rates, the mist concentration, and the ignition energy and duration, was ensured by a specifically customized control system guaranteeing the flexibility and compliance of the test apparatus. The droplet size distribution (DSD) and the level of turbulence of the JetA1 mist cloud were first determined by an in-situ laser diffraction sensor and by Particle Image Velocimetry, respectively. The lower explosive limit (LEL), the minimum ignition energy (MIE), the limiting oxygen concentration (LOC), the

maximum explosion overpressure (P_{max}), and the maximum rate of pressure rise (dP/dt_{max}) were then determined for different mist concentrations, ambient temperatures, initial turbulence levels, energies, and DSD.

Tests showed that the LEL_{mist} of JetA1 mists of an average diameter of 8 μm is around 94 g/m^3, a value which increases to 220 g/m^3 with increasing DSD. This value also tends to decrease considerably with increasing temperatures. Moreover, at a JetA1 concentration of 125 g/m^3, P_{max} and dP/dt_{max} as high as 6 bar and 192 bar/s respectively were reached, the latter increasing to about 480 bar/s at T = 60 °C. These mists were shown to be ignitable using energies as low as 200 mJ, which is lower than that of vapors at low temperatures, and a limiting concentration of oxygen of 15.8 $\%_{v/v}$. The potential presence of hydrocarbon mist should therefore be an element that requires reconsidering the classification of hazardous areas. Finally, to stress the influence of the vapor-liquid ratio present in the cloud before ignition on the combustion kinetics, an evaporation model based on the d^2-law was developed estimating the evaporation time and the vapor quantity at different initial temperatures or droplet diameters.

Findings were shown to be well coherent allowing the proposition of a new technique for determining hydrocarbon mist safety criteria. Finally, results have shown that JetA1 mists can ignite at temperatures below the liquid's flashpoint under varying turbulence levels and droplet size distributions.

Keywords

Fuel mist, aerosol explosion, hydrocarbons, flammability, risk assessment, hazardous areas, explosive atmospheres, kerosene

Nomenclature

α	Significance level	P_{max}	Maximum explosion overpressure
B_T, B_M	Thermal and mass transfer Spalding numbers	*PIV*	Particle Image Velocimetry
CEA	Chemical Equilibrium with Applications	*Q*	Combustion enthalpy
C_p	Heat capacity	*r*	Droplet radius
d_o	Orifice diameter	*Re*	Reynolds number
DSD	Droplet size distribution	ρ	Density
dP/dt_{max}	Maximum rate of pressure rise	*s*	Skewness
d_x	Representation diameter where x% of the distribution has a smaller droplet size	*Sc*	Schmidt number
Δ	Span factor	*SMD*	Sauter mean diameter
E(t)	Expected value of the quantity *t*	*T*	Temperature
Φ	Fuel equivalence ratio	t_{inj}	Injection time
HAC	Hazardous Area Classification	*u, v*	Horizontal and vertical velocity
k	Kurtosis	*v*	Velocity
K	Evaporation rate constant	*V*	Initial jet velocity
La	Laplace number	*We*	Weber number
LEL	Lower explosive limit	x_i	Molar fraction of species *i*
Le	Lewis number	*Y*	Mass fraction
LOC	Limiting Oxygen Concentration	***Indices***	
L_v	Enthalpy of vaporization	*l*	Liquid
λ	Thermal conductivity	*g*	Gas / air
μ	Viscosity	*v*	vapor
MIE	Minimum ignition energy	*d*	droplet
$\dot{m}$	Mass flowrate	*s*	Stoichiometry
N	Number of droplets	*rms*	Root-mean-square
Oh	Ohnesorge number	∞	Surrounding gas environment

1 Introduction

Fortunately, explosions are rare but frequently destructive and are subject to sustained attention during risk analyses. Therefore, the attention of prevention officers and legislators has long been focused on the risks presented by the generation of clouds of flammable vapors or gases, as well as on the dispersion of combustible powders. However, accidental explosions are not limited to these two states of matter, solid and gas, and liquids dispersed as mists can also cause explosions.

In process safety, the identification of hazards related to the potential generation of mists is much less straightforward than for gases and vapors. Thus, the mere presence of the liquid is not sufficient to consider an explosive atmosphere and both the conditions of dispersion and the nature of the fluid play key roles. In a mist, the liquid phase cannot obviously explode by itself, and the presence of a sufficient gas phase is compulsory to trigger the explosion. Nevertheless, even mists of high-flashpoint fuels can provoke explosions. In fact, such fuels are usually classified as non-hazardous but can result in hazardous explosions once stored or handled under pressure [1]. For instance, ruptures in vessels and pipelines can occur due to accidental damages or corrosion. Another example is the eventual evaporation of fuels in heated areas, their subsequent circulation, and their condensation in colder areas [2]. Such unplanned formations of flammable hydrocarbon aerosols make chemical and petrochemical industries prone to explosion hazards. A considerable number of mist explosions have been reported throughout the years despite the efforts to mitigate such incidents. For instance, an incident survey was published by Santon [3] reporting 37 mist incidents, among which 9 explosions lead to 29 fatalities. Ten years later, Lees et al. [4] analyzed incident databases to institute common trends in flammable mists incidents. The authors' findings demonstrated that around 10% of reported releases on offshore oil and gas installations in the United Kingdom involved sprays or mists.

A simple analysis of experience feedback is not sufficient to control these accidental phenomena and researchers have been interested in this topic for a long time, and as early as 1955, Eichhorn clearly addressed this issue in an article entitled "Careful! Mist can explode" [5]. Since then, the prospect of mists igniting at temperatures well below their flashpoints has been introduced. A few years later, Burgoyne discussed mist and spray explosions and measured the effect of drop size on the flammability of mists [6,7]. Naegeli and Weatherford issued a report in which they stated that the presence of fuel mist plays an important role in the

initiation and the propagation of a flame, for both low and high-volatility fuels such as aviation kerosene and gasoline, respectively [8]. The authors also stressed that the physical and chemical processes in such incidents are 'among the least studied and understood in all combustion phenomena'. Studies focusing on the generation, ignition, combustion, and explosion of flammable mists were reviewed by Eckhoff in a literature survey in 1995 [2]. Since then, there has been a consistent increase in interest in such a vital topic. More recently, a comprehensive review was presented by Yuan et al. [9] who proposed a systematic strategy to examine aerosol explosions.

Of frequent occurrence in the industry, causing major accidents and being increasingly documented, such explosive mists are neither well classified nor subject to dedicated regulations. For instance, the Energy Institute [10] defines hazardous area classification (HAC) as an essential part of risk assessment in order to identify hazardous and non-hazardous areas near equipment storing or handling of flammable fluids in industrial sectors such as production, processing, distribution, and retail sectors. However, EI 15 clearly highlights the lack of knowledge on such a subject by stating that "there is little knowledge on the formation of flammable mists and the appropriate extents of associated hazardous areas". In fact, industry codes of practice are already available for use in industries concerning hazards and explosions linked to gas or dust releases; however, mists or sprays are often disregarded, and standards for such cases have not been completely set yet. More precisely, the threat of the formation and ignition of explosive atmospheres (ATEX), notably linked with the generation of a flammable mist, must be assessed under European ATEX standards. Risk analysis and area classification, however, are currently complex due to a lack of both knowledge and standard test procedures.

Therefore, identifying factors and measures of liquid handling, and determining fluids' safety parameters, such as their ignition sensitivity and/or explosion severity, will be helpful to assess the explosion risk of hydrocarbon mists. Indeed, explosion severity parameters help in

designing suitable safety equipment as advised by the ATEX directive 2014/34/EU [11] and proper explosion prevention and protection systems. In addition, determining the Minimum Ignition Energy (MIE), an ignition sensitivity parameter, can help control electrostatic hazards by limiting the current and voltage in a circuit, properly earthing/grounding, etc. Similarly, the Lower Explosive Limit (LEL) is of great importance as it helps ensure that a release be maintained below this threshold to avoid hazardous scenarios. The Limiting Oxygen Concentration (LOC) is also a vital parameter that is useful to inert an explosive atmosphere when process condition adjustments fail to preserve substances out of the explosive range. For all these safety parameters, there is currently no standard describing how to assess them quantitatively. There is no clearly identified experimental equipment or device for this task, nor are there any defined operating protocols. The ability to determine such parameters is a steppingstone to the classification of hazardous areas (HAC) and the improvement of current ATEX standards and regulatory provisions concerning liquid aerosols. The original aim of our research is to provide a single device and a set of protocols to easily determine the above safety parameters.

To illustrate this approach, this study focuses on the flammability and explosivity of kerosene Jet A1 mists. This fuel was chosen due to its ongoing involvement in explosion hazards despite the efforts taken to reduce its flammability and its ability to disperse. For instance, Santon [3] demonstrated that seven incidents out of 37 detailed in their review were associated with kerosene mists. Most of which involved transportation activities, notably cargo accidents and aviation kerosene explosions. One marked disaster involving aviation fuel was the September 11th terrorist attacks in which, according to Maragkos and Bowen [12], the high-momentum impact and subsequent rupture of the fuel vessels were the reason behind the generation of the pressurized release of aviation fuel. Furthermore, Willauer et al. [13] stressed the risks behind the high flammability and extreme explosivity of atomized jet fuel-air mixtures. The authors'

study focused on finding chemical methods (test of a series of additives) for decreasing jet fuel flammability. Bowen and Shirvill [1] also highlighted the dangers associated with kerosene atomization. It should also be noted that unfortunate incidents continue to take place and sometimes remain unreported in low- and middle-income countries where kerosene is still being used as a household fuel. Moreover, filling or emptying fuel reservoirs (voluntarily or inadvertently) must also be carefully evaluated for the creation of aerosols. Kerosene explosions took place in Cilacap (1995) and Mombasa (2013) due to tank refueling and storage leaking, respectively.

In this study, Jet A1 mists were tested in a new apparatus based on the standardized 20 L explosion sphere. An original system allowing the control of both the concentration and the Droplet Size Distribution (DSD) has been developed. The spatial distribution of the velocity and the turbulence of the generated mist were characterized by Particle Image Velocimetry (PIV). Explosion tests were conducted to study the mist explosion sensitivity by determining the lower explosivity limit (LEL), the limiting oxygen concentration (LOC), and the minimum ignition energy (MIE). Moreover, the maximum explosion overpressure (P_{max}) and the maximum rate of pressure rise (dP/dt_{max}) of Jet A1 mists were determined in the same vessel. In addition, tests were carried out to study the influence of some operating conditions (DSD, temperature, ignition energy) on the safety parameters. Experimental results were finally exploited in an evaporation model and compared to theoretical results obtained by the NASA computer program Chemical Equilibrium with Applications (CEA). These steps allow establishing that it is indeed possible to characterize the flammability and explosion severity of mists in a single set-up such as the modified 20 L sphere.

2 Materials and methods

2.1 Fuel properties

Mist explosion incident reviews report a considerable variety of involved fuels ranging from vegetable oils to hydraulic oils and crude oils [2–4]. The Health and Safety Executive (HSE) led an oil mists Joint Industry Project (JIP) during which a list of fluids was proposed comprising fuels of industrial interest and specific physicochemical properties (lubricating oil, hydraulic oil, light and heavy fuel oil, jet fuel, diesel, biodiesel, vegetable oil, heat transfer fluids, transformer oil, process fluids, white spirit). A flammable mist classification system was presented in order to estimate the tendency of a liquid to form a flammable mist. In this system, two parameters were used: the liquid ignitability, represented by its flashpoint, and the tendency of a liquid jet to atomize into droplets when released from a nozzle orifice. The atomization behavior was characterized using two empirical correlations based on the primary (Ohnesorge) and secondary (Brodkey) break-up [14]. All calculations were performed at a standardized set of conditions: a 10-bar release from a 1 mm orifice. Burrell and Gant [14] published a report demonstrating the followed calculations to classify the liquids listed above in the flammable mist classification system. These calculations led to the diagrammatic classification of the fluids into four release classes. In the general framework of this study, a variety of fluids (ethanol, isooctane, diesel, kerosene, light fuel oil, hydraulic oil, and biodiesel) was chosen to represent these release classes.

As conveyed in the introduction, due to its industrial interest, this article will focus on the results obtained with Jet A1, which was also listed in the HSE liquid classification. There exist numerous types of jet fuels used in various applications (Jet A, Jet B, Jet A1, JP-8, etc.). Most international aviation companies use Jet A1; however, Jet A is used in the United States. According to Dagaut and Calhonnet [15], the most significant difference between Jet A1 and

Jet A is the freezing point, as it is – 40 °C for Jet A and – 47 °C for Jet A1. It should be stressed that Jet A1 specifications are defined using minimum/maximum values or range of properties, which implies a certain variability of properties depending on the fuel supply.

Table 1 lists the main physicochemical properties of Jet A1 as well as the HSE release class representation for Jet A1. It should be noted that some properties were measured as fuel aging, petroleum cuts, and sources can all affect initial values or those indicated in safety data sheets. The Hoeppler Falling-Ball Viscometer (Brookfield KF30 model) was used to measure the dynamic viscosity in accordance with DIN 53015. Surface tension measurements were also carried out using the Pendant Drop technique. Moreover, the Setaflash Series 3 flashpoint apparatus was used to test the flashpoint per the ASTM D3278-96 standard. It should be stressed that in order to meet the specifications of Jet A1, the flashpoint must be above 38°C, which is demonstrated here. Other physicochemical properties were deduced from the MSDS of the supplier. Finally, the HSE Release Class was determined based on the Ohnesorge number (Oh), which is the ratio between viscous forces to surface tension and inertial forces. Therefore, at a fixed Reynolds number, increasing Oh will improve liquid atomization.

Table 1: Physicochemical properties of Jet A1 († MSDS from Neste)

	Jet A1*
Measured density (kg/m^3)	840
Measured flashpoint (°C)	40
Measured surface tension (kg/s^2)	0.026
Measured dynamic viscosity (mPa.s)	1.2
HSE Release Class	Release Class I (Oh ratio ≥ 2, Flashpoint < 125°C)
Auto-ignition temperature (°C)	250 †
Flammability limits (%)	0.6 - 6 †
Vapor pressure (kPa)	~ 2 (at 38 °C) †

Initial boiling point and range (°C)	130 - 300 †

2.2 Mist generation system

Explosively flammable mist clouds, which are accidentally formed, can be caused by several phenomena. Predicting the properties and behavior of a mist cloud before its release proves to be difficult because ruptures or leaks in a vessel have very uneven shapes and may occur in different conditions. To better predict the flammability and explosivity of mist, tests should be performed in the closest conditions possible to industrial accidents. There exists a wide range of ways used to generate such mists. For instance, according to Gant [16], four principal methods are used: spray discharge from a pressurized liquid reservoir, condensation of saturated vapor, agitation and splashing, and air stripping. In addition to the four listed ways, electrospray was used notably by Lin et al. [17] for aerosol generation and the analysis of flame propagation. Each generation method has both advantages and disadvantages. However, it is necessary to take into account that the suggested experimental approach for determining and characterizing the ignition sensitivity and explosion severity of mists is intended to be standardized, allowing results to be compared and generic safety measures to be proposed. As a result, the chosen generation system should be easy to find and implement while also simulating “idealized” conditions of a mist release.

For this study, a siphon gravity-fed spray generation system was used. This system comprises a Venturi junction with two inlets: a pressurized air inlet connected to a compressed air cylinder and a liquid inlet connected to the fuel reservoir maintained at room temperature (Figure 1). A mist/spray generation system of the siphon type usually comprises two key components (Spraying Systems): a fluid nozzle, which ensures fuel intake, as well as an air cap, through which the liquid/air jet passes and fragments. Both nozzles/caps were altered in order to change the flow rate and the droplet size distribution of the mist cloud, hence changing the initial conditions. Figure 2 shows the three nozzle air caps of different orifice diameters (two extremities and one intermediate diameter) chosen for this study. Aside from the nozzle set, the air injection pressure, which has a significant impact on the droplet size, was changed between 2 and 5 bar. These pressures were chosen based on the maximum pressure tolerance of the three nozzle sets.

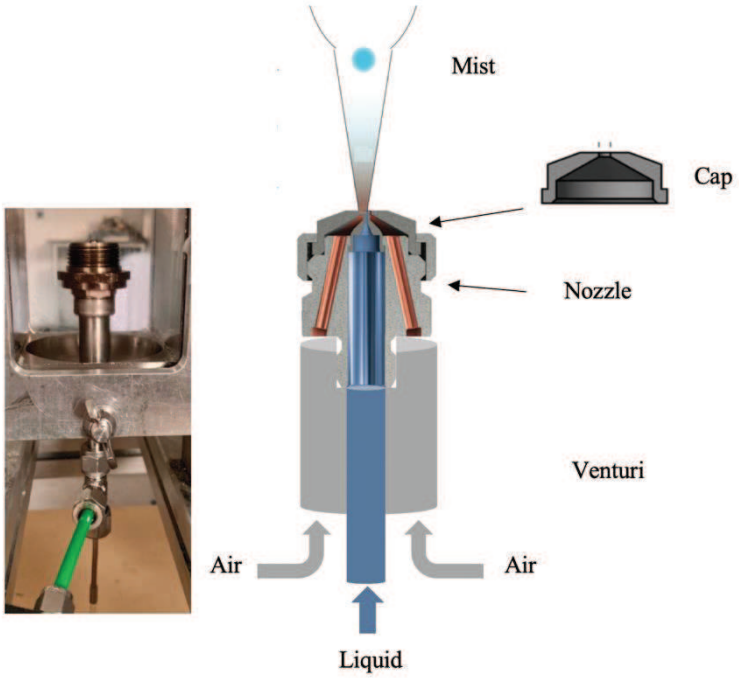


Figure 1: Mist generation system based on a Venturi junction (elements from Spraying Systems®)

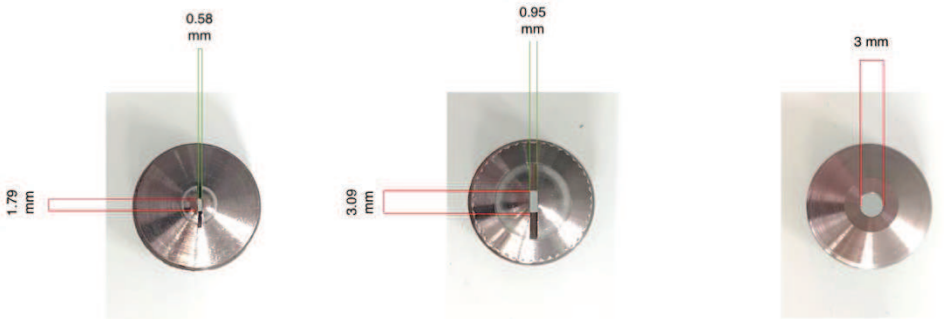


Figure 2: Three air caps for nozzle sets and their denomination: (a) N1, (b) N', (c) N2

2.3 The Modified 20 L Ignition and explosion Severity Test device (The MIST Sphere)

To adapt the standard 20 L explosion sphere, notably used for dust explosion tests, to mist explosion tests, modifications were made as seen in Figure 3. For instance, as mentioned by El-Zahlanieh et al. [18], the mist generation system detailed in section 2.2 was installed at the bottom of the sphere, the dust container was removed, and two electronic valves were installed to control the inlet flow rates (gas and liquid) as well as the liquid/air ratio. A check valve was placed between the venturi and the fuel inlet valve to prevent backflow during the explosion phase.

Ignition sensitivity and explosion severity tests were both performed in the 'MIST sphere'. During each test, the sphere was first partially vacuumed to a calculated pressure before injecting the fuel/air mixture. This ensured that atmospheric pressure was reached when the mist was fully injected. This pressure was calculated based on the fixed injection time which can be varied depending on the mist concentration needed inside the vessel. The injected mass was measured by a mass balance tracking its evolution with the injection time. The temperature of the sphere was controlled with a water jacket avoiding the sphere heating between two tests. To ignite the generated mists, one of the two ignition sources mentioned in section 2.5.1 (spark

or chemical igniters) was used. The apparatus was controlled, and data was collected using a new control system and a LabView program developed by the LRGP. With an acquisition frequency of 5000 measurements per second, this system manages the KSEP 310 (control unit – bypassed and mainly used for injecting compressed air, vacuuming the sphere, and actuating the chemical ignitors), KSEP 320 (high voltage unit for a permanent spark ignition), and KSEP 332 (data acquisition unit) units (Cesana AG), the inlet electronic valves, and ensures safe operation of the test equipment and optimal interpretation of the explosion findings.

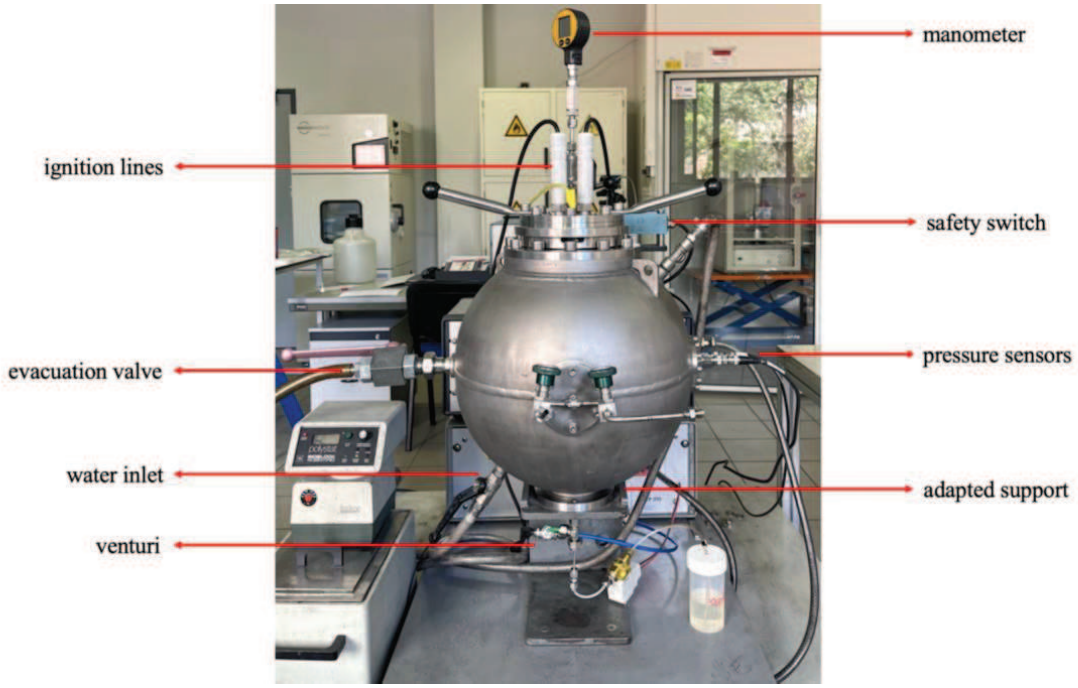


Figure 3: The Modified 20 L Ignition and explosion Severity Test device

2.4 Mist characterization

Mist characterization is a mandatory step to take while studying the flammability of oil mists. Gant et al. [16] stated that properly characterizing a mist before its ignition is crucial since the droplet size distribution, the concentration, and the turbulence of mists can considerably influence their safety parameters. Moreover, Bowen and Cameron [19] expressed the need to quantify particle sizes, total equivalence ratio, droplet equivalence ratio, and pre-ignition turbulence for aerosol fuel clouds. The authors also stressed the importance of temporal resolution for used characterization techniques. Lemkowitz and Pasman [20] correspondingly stated that the DSD is the most important physical property that influences explosion parameters. According to the authors, turbulence is also a property that has a complex effect on mist explosions.

To characterize the mist cloud generated in the 20 L sphere, generation studies were performed as a function of three relevant parameters: the nozzle type, the spraying pressure (or air pressure), and the fluid properties. The injection time was fixed to obtain comparable results as

the three parameters were varied. The DSD was studied using an in-situ laser diffraction sensor. As for the spatial distribution of the velocity and the turbulence, they were quantified by applying Particle Image Velocimetry (PIV).

2.5.1 Droplet Size Distribution (DSD)

An in-situ laser diffraction sensor (Helos/KR-Vario by Sympatec GmbH), based on the Fraunhofer diffraction theory (FREE, parameter-free Fraunhofer evaluation), was used to assess the time evolution of droplet size distributions. The experimental vessel used was a replica of the 20 L sphere with transparent windows (borosilicate glass) on each side to allow visual access [21]. The Helos laser sensor measures the DSD directly through the transparent windows using three high-resolution measuring ranges (R1, R3, and R5) from 0.5 µm to 875 µm. During this study, the droplets were assumed spherical (if necessary, it is possible to modify the shape factor in the mentioned apparatus) denoting that, regardless of stresses and particle orientation, the measured diameter remains the same. The R3 lens was mainly used as it covers a range of droplet diameters, from 0.5/0.9 µm to 175 µm, which correspond to those generated by the three nozzle sets. The acquisition frequency was set to 2 distributions per millisecond. d_{10}, d_{50}, $d_{90,}$ and $D_{3,2}$ (Sauter Mean Diameter, SMD) are among the measurements provided by the sensor. The height of the sensor was set to match the location of the ignition source (i.e., the center of the sphere), to assess the DSD of the mist just before ignition.

Influencing factors

There exist various factors that can affect and alter the characteristics of a spray. For instance, Kooij et al. [22] studied the effect of spraying parameters, such as the injection pressure and the nozzle type, as well as fluid parameters, such as the liquid viscosity and the surface tension, on the characteristics of sprays, more specifically on the droplet size. Their findings showed that the size of droplets is determined by a competition between fluid inertia and surface tension. They, therefore, concluded that it is possible to predict the droplet size from the calculation of

the Weber number and the geometry of the nozzle. Moreover, Schick [23] listed the following factors: fluid characteristics, fluid viscosity, the spray nozzle design, the flow through the spray nozzle, and the air pressure in the case of two-fluid nozzles, as factors based on which the droplet size and the droplet size uniformity tend to vary.

A full factorial design of experiments was applied to study the influence of the factors mentioned in the paragraph above. The three nozzle sets were used to generate mists at four different injection pressures: 2, 3, 4, and 5 bar. Moreover, six fluids of different surface tensions, viscosities, and densities were tested under fixed conditions (iso-octane, ethanol, diesel, light fuel oil, biodiesel and kerosene), which allows to cover a wider range of application and not to be limited to Jet A1. DSD measurements were performed during a four-second-generation period and up to 1 second after the valves' closure, with intervals of 50 ms (2 DSD per millisecond and an average value each 50 ms). Experimental data were subsequently analyzed using a MATLAB program and the Minitab Statistical Software. Reproducibility tests were carried out in the center of the study area defined by the design of experiments, which made it possible to determine the standard deviation. The significance level of the tests was set at 0.05. Pareto charts of standardized effects were used to determine the magnitude and the importance of the effects of the three chosen factors (the nozzle orifice diameter, the air injection pressure, and the type of fluid) on the five chosen parameters to be studied (mean diameters d_{10}, d_{50}, d_{90}, SMD, the span factor, skewness, and kurtosis). A dimensional analysis, followed by multiple linear regression, was also applied, highlighting these influences (Section 3.1).

The measured Sauter Mean Diameter is calculated as follows:

$$D_{3,2} = \frac{\sum N_i D_i}{\sum N_i D_i^2} \quad (1)$$

d_{50} represents the diameter below which 50% of the total liquid volume constitutes droplets of smaller diameter, the same thing goes for d_x where x represents the percentage of such droplets. However, the median diameter by itself is not sufficient to reflect a true size distribution as it can be misleading, especially in the case of diameters of ranges over two or more orders of magnitude [24]. Lefebvre and McDonell [25] also state that a droplet size distribution cannot be defined by one single parameter. Therefore, to complement d_{50}, the representative diameters d_{10}, d_{90}, and SMD were also measured. In addition, the span factor, the skewness, and the kurtosis were calculated from input data consisting of the distribution.

a) Span Factor: this parameter provides an indication of the range of the droplet sizes relative to the median diameter. It represents the polydispersity of a droplet size distribution. Its calculation equation is:

$$\Delta = \frac{d_{90} - d_{10}}{d_{50}} \tag{2}$$

b) Skewness: this parameter measures the level of asymmetry of a distribution curve around the mean value. If its value is positive, this means that the data spreads out more to the right of the mean than to the left and vice versa. Its calculation equation is:

$$s = \frac{E(x-\mu)^3}{\sigma^3} \tag{3}$$

c) Kurtosis: this parameter indicates whether the data are light-tailed or heavily tailed relative to a normal distribution. A value of 3 corresponds to a normal distribution. Values less than 3 represent a distribution that is less outlier-prone than the normal distribution and vice versa. Its calculation equation is:

$$k = \frac{E(x-\mu)^4}{\sigma^4} \tag{4}$$

Where μ is the mean of x, σ is the standard deviation of x and $E(t)$ represents the expected value of the quantity t.

2.5.2 Particle Image Velocimetry (PIV)

Under particular conditions, Particle Image Velocimetry was performed to determine the level of turbulence reached by a mist generated in the MIST sphere. In fact, the level of violence of an explosion is considerably affected by the turbulence of the mixture. To conduct these tests, a continuous wave laser sheet with a wavelength of 532 nm was emitted using Neodym-Yttrium-Aluminum-Garnet (Nd:YAG). The dispersed droplets would then be lighted up, allowing their movement to be followed. The flow of the droplets was recorded with a high-speed video camera (Phantom VEO 410L) at 2000 frames per second. The experimental set-up is displayed in Figure 4. PIVlab 2.45 was then used to conduct image preprocessing, PIV analysis utilizing interpolation techniques, calibration, post-processing, and data validation on the recorded videos [26] (see Figure 5). The mean velocities $\bar{u}$ and $\bar{v}$, as well as the horizontal and vertical velocity fluctuations u_i' and v_i' (equations 5 and 6), were estimated from the data collected from PIVlab, allowing the calculation of the root-mean-square velocity (v_{rms} – equation 7), which physically portrays the turbulence kinetic energy.

$$u_i' = u - \bar{u} \tag{5}$$

$$v_i' = v - \bar{} \tag{6}$$

$$v_{rms} = \sqrt{\frac{1}{N}\sum (u_i')^2 + \frac{1}{N}\sum (v_i')^2} \tag{7}$$

where u_i' is the horizontal velocity fluctuation, v_i' is the vertical velocity fluctuation and N is the number of droplets detected for the velocity estimation.

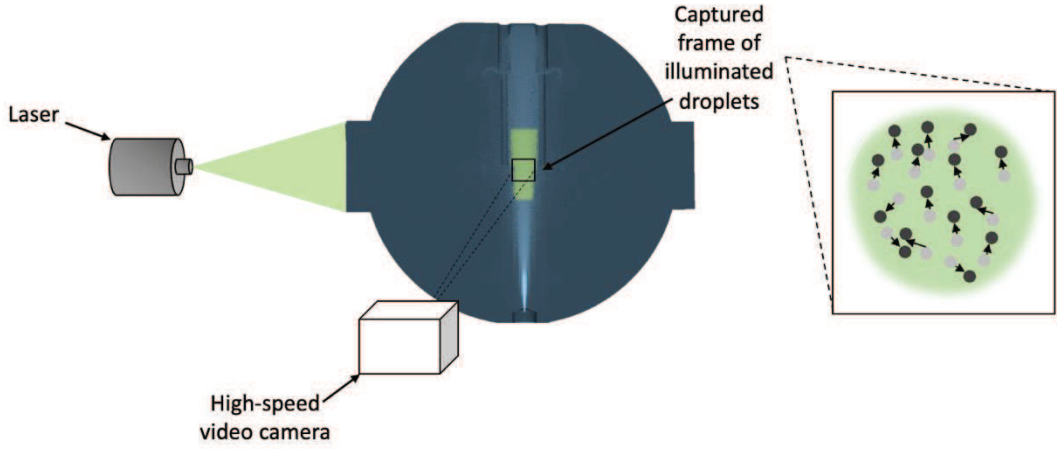
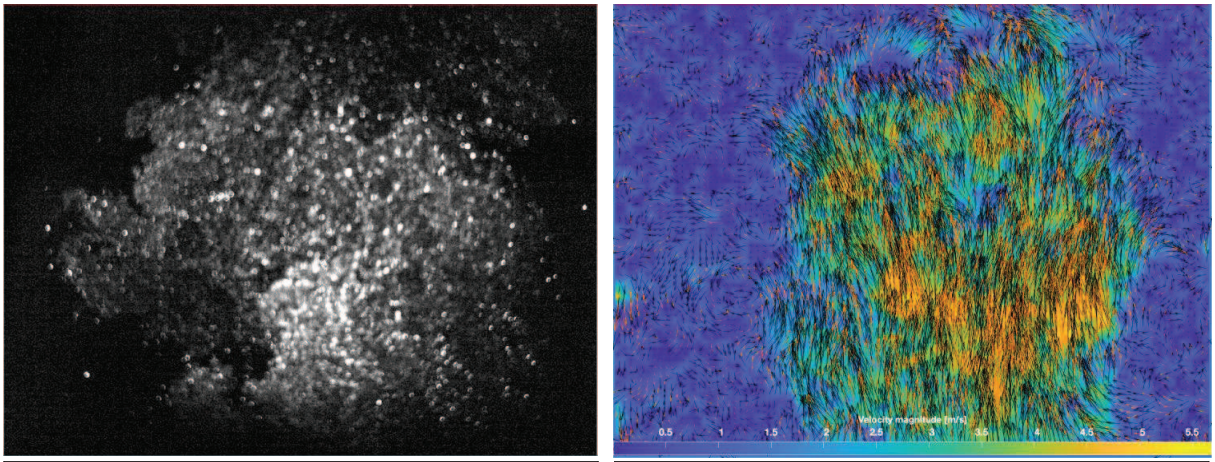


Figure 4: Particle Image Velocimetry experimental set-up with the 20 L open sphere



Illuminated droplets – Image pre-processing | Post-processing: velocity magnitudes

Figure 5: Left: pre-processed imaged of illuminated kerosene droplets – Right: spatial variation of the velocity magnitude (from 0 to 5 m/s) of kerosene droplets at the end of the generation using nozzle set N1 and P_{inj} = 3 bar

2.5 Mist explosion sensitivity and severity tests

The mist explosion tests were performed in the sphere described in Section 2.3. Ignition sources were used according to the type of test performed and the energy requirements. To determine the explosion thermo-kinetic parameters, the maximum explosion pressure (P_{max}) as well as the maximum rate of pressure rise (dP/dt_{max}), a MATLAB program was prepared using both two-point and five-point derivatives and in agreement with the European standard EN 15967:2022

[27] “Determination of the maximum explosion pressure and maximum rate of pressure rise of gases and vapors”. Tests were performed immediately after injection, which means that the ignition system was actuated just after the generation of the mist cloud inside the sphere.

Under certain conditions, both the explosion severity and sensitivity were studied to characterize the explosibility of the Jet A1 mist cloud. Testing conditions (turbulence levels, droplet size distribution, and concentrations) were chosen to represent and cover a wide range of industrial leaks. Additionally, the NASA computer program Chemical Equilibrium with Applications (CEA) [28] was utilized to compare experimental data to theoretical liquid or gas phase combustion models. CEA also permits obtaining the composition of the equilibrium products of a combustion reaction.

2.5.1 Ignition sources

Accidental fires or explosions can be caused by a series of potential ignition sources varying from sparks or electrical discharges to hot surfaces or malfunctioning electrical circuits. Several ignition sources, such as exploding wire ignitors, spark ignition, pyrotechnical ignitors, and hot spot ignitors, have been employed in past investigations on explosion limits and deflagration pressures.

Both spark ignition, as well as chemical pyrotechnical ignitors, were used in this study. The need for energies starting from 100 mJ and going to 10 kJ justifies the choice of these two ignition sources. In fact, the spark ignition used delivers a maximum power of 225 W, i.e., 225 J/s. Thus, a permanent spark would be generated during 444 milliseconds to deliver an energy of 100 J. Therefore, for energies ranging from 100 J to 10 kJ, in order not to generate for a long duration and cause the droplets to sediment, chemical pyrotechnical ignitors (Sobbe GmbH) were used, which is especially in accordance with EN 14034 standards. Both ignition sources were placed in the center of the MIST sphere. The spark tungsten electrodes were

placed with a separating distance of 6 ± 0.1 mm on stainless-steel electrodes which were insulated from the sphere's wall using Teflon plugs. The permanent spark was generated following a signal sent from the KSEP 320 high voltage unit which was connected to the electrodes. To control the generation time, hence the ignition energy, the unit was bypassed by a custom control system. The chemical pyrotechnical ignitors were connected as shown in Figure 6 to the stainless-steel electrodes. A low-voltage electrical signal was supplied by the KSEP 310 unit to actuate these ignitors. As the use of a specific ignition source varies with the application, both ignition sources were examined at 100 J to guarantee that they both provide similar results (Section 3.3).

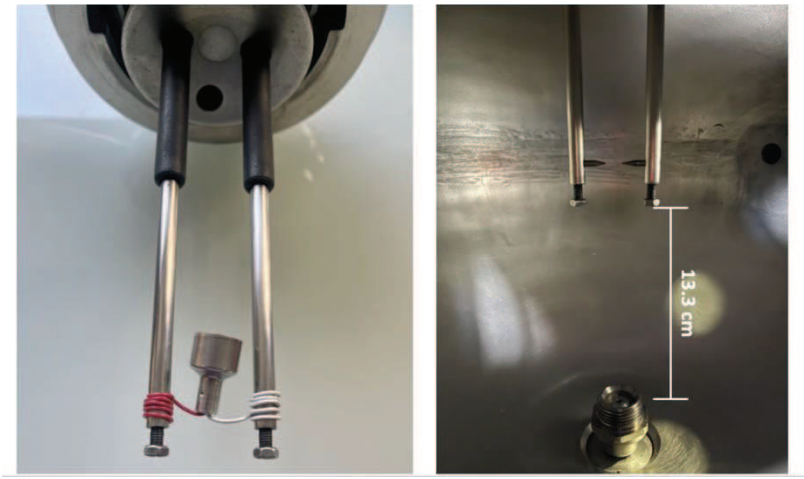


Figure 6: Ignition sources placed on the two stainless-steel electrodes of the 20 L sphere; right: chemical ignitors, left: spark ignition

3 Results and discussion

After having characterized the mists in terms of granulometry and turbulence, an evaporation model allowing to determine the quantities of vapor and liquid present in the explosion sphere before ignition will be developed. Then, the results of the explosion tests will be commented on.

3.1 Droplet Size Distribution (DSD)

To measure the range of diameters that could be covered using the three nozzle sets, Jet A1 mists were generated into the modified 20 L open sphere at ambient temperature during 4 s and an injection pressure of 3 bar (pressure used for the following explosion experiments). Measurements were performed with intervals of 50 ms (2 DSD per millisecond and an average value each 50 ms) and were stopped 1 second after the closure of the inlet valves. Figure 7 demonstrates that, with the three chosen nozzle sets, three droplet diameter ranges are attainable. Nevertheless, it should be noted that a peak corresponding to small diameters (between 10 and 15 µm) was observed for both nozzle sets N' and N2. In the case of nozzle set N', the peak observed was explained by the persistence of 'primary droplets' combined with a coalescence phenomenon for larger drops (around 25 µm), whereas, in the case of nozzle set N2, the peak appears after a certain time of generation signifying a fragmentation phenomenon.

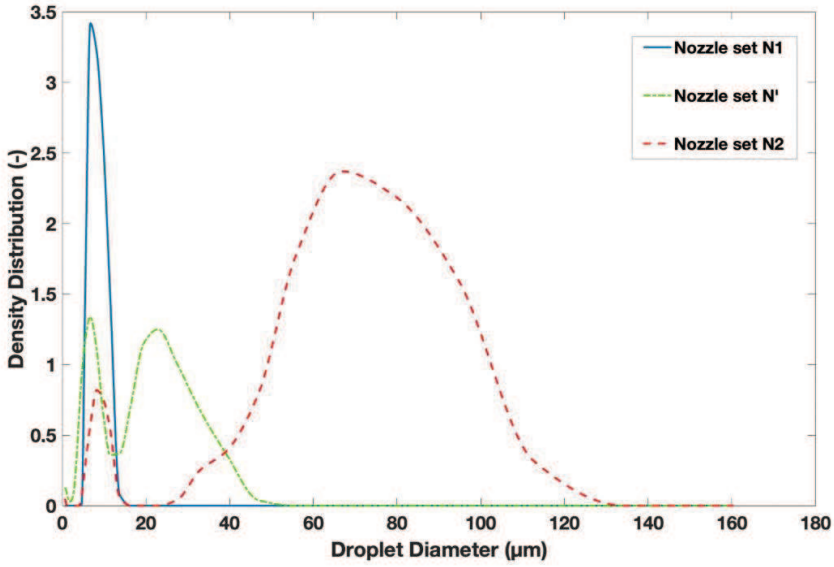


Figure 7: Droplet size distribution (volume/mass) at t = 4000 ms of Jet A1 mist generation at P = 3 bar using the three nozzle sets

Once the 3 ranges of diameters were validated, the evolution of the Jet A1 DSD with time was studied. Jet A1 mists were generated into the open sphere using nozzle set N2 with an injection pressure of 3 bar. The time employed for measuring the diameter ranges (4 s generation) was also used to measure the time evolution of droplets. Figure 8 presents distributions starting from t = 1950 ms corresponding to the beginning of the second half of the generation step, and ending at t = 3950 ms, corresponding to 50 ms before the closure of the injection valves. A time-step of 400 ms was used in order not to overload the figure. As it can be seen, the peak corresponding to primary droplets of a median diameter of 8 µm persisted all along the last 2 seconds. However, this peak tends to decrease in height (the log density distribution decreases from about 1.5 to 0.75). A shift towards the large diameters was also observed with increasing time showing the likely presence of a coalescence phenomenon. Nevertheless, it should be stressed that the time-evolution of the DSD does not call into question the validation of the 3 ranges of diameters.

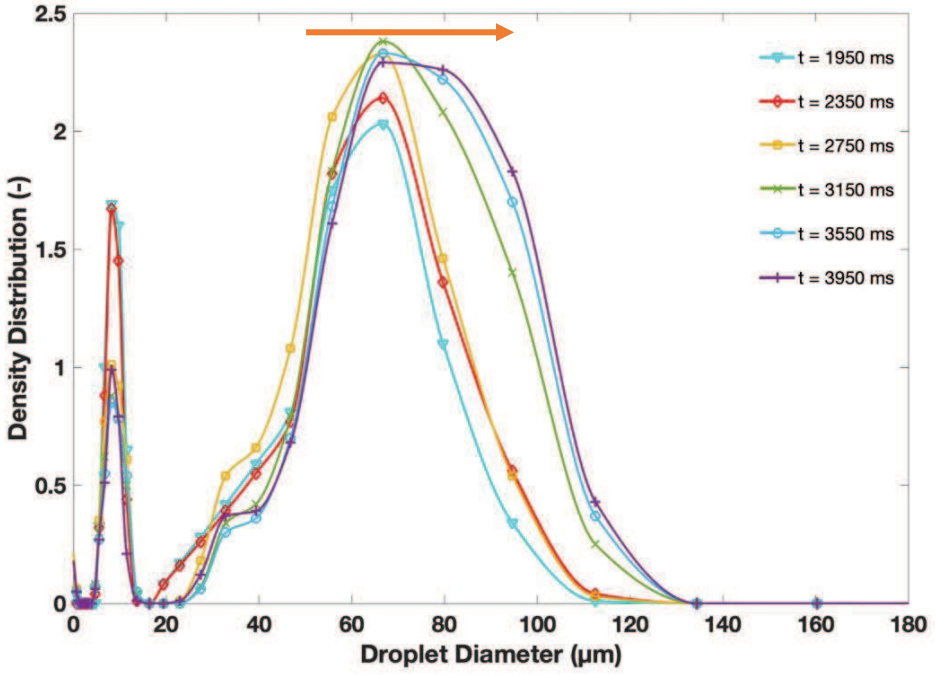


Figure 8: Droplet size volume / mass distribution of Jet A1 mists generated at P = 3 bar using nozzle set N2 - time step 400 ms starting from t_{inj} = 1950ms

Table 2 also demonstrates the evolution of d_{10}, d_{50}, d_{90}, and SMD diameters after stopping the injection and without any effect from the injection of air. A slight increase (a maximum of 8% of the initial value) in the four diameters was observed justifying the shift of the distribution curves to the right and confirming the coalescence hypothesis. Moreover, the span factor, skewness, and kurtosis of each distribution curve were calculated. The span factor, which quantifies the distribution width, remained constant at a value of 1.4, showing that the distribution around the mean diameter did not vary a lot in the last second of measurement. Similarly, change in the values of skewness and kurtosis can be considered as negligible, demonstrating that, other than a change in mean diameters, the distribution curves do not change considerably after stopping the injection and that the mist cloud remains rather stable before ignition occurs.

Table 2: Variation of droplet size parameters as a function of time

time (ms)	d_{10} (µm)	d_{50} (µm)	d_{90} (µm)	SMD (µm)	Span factor	Skewness	Kurtosis
t_f – 50 ms	7.3	58.6	90.4	15.6	1.41	1.76	5.01
t_f + 150 ms	7.6	60.5	92.3	16.7	1.39	1.81	5.16
t_f + 350 ms	7.6	61.2	93.8	16.5	1.40	1.80	5.10
t_f + 550 ms	7.7	61.9	94.3	17.4	1.39	1.75	4.92
t_f + 750 ms	7.7	62.2	95	16.6	1.40	1.77	4.93
t_f + 950 ms	7.7	63	96.3	16.9	1.40	1.81	5.06

A full-factorial design of experiments was implemented to study the effect of the influencing factors listed in Section 2.4.1. Pareto charts, showing the absolute values of standardized effects, from the largest to the smallest, are presented in Figure 9.

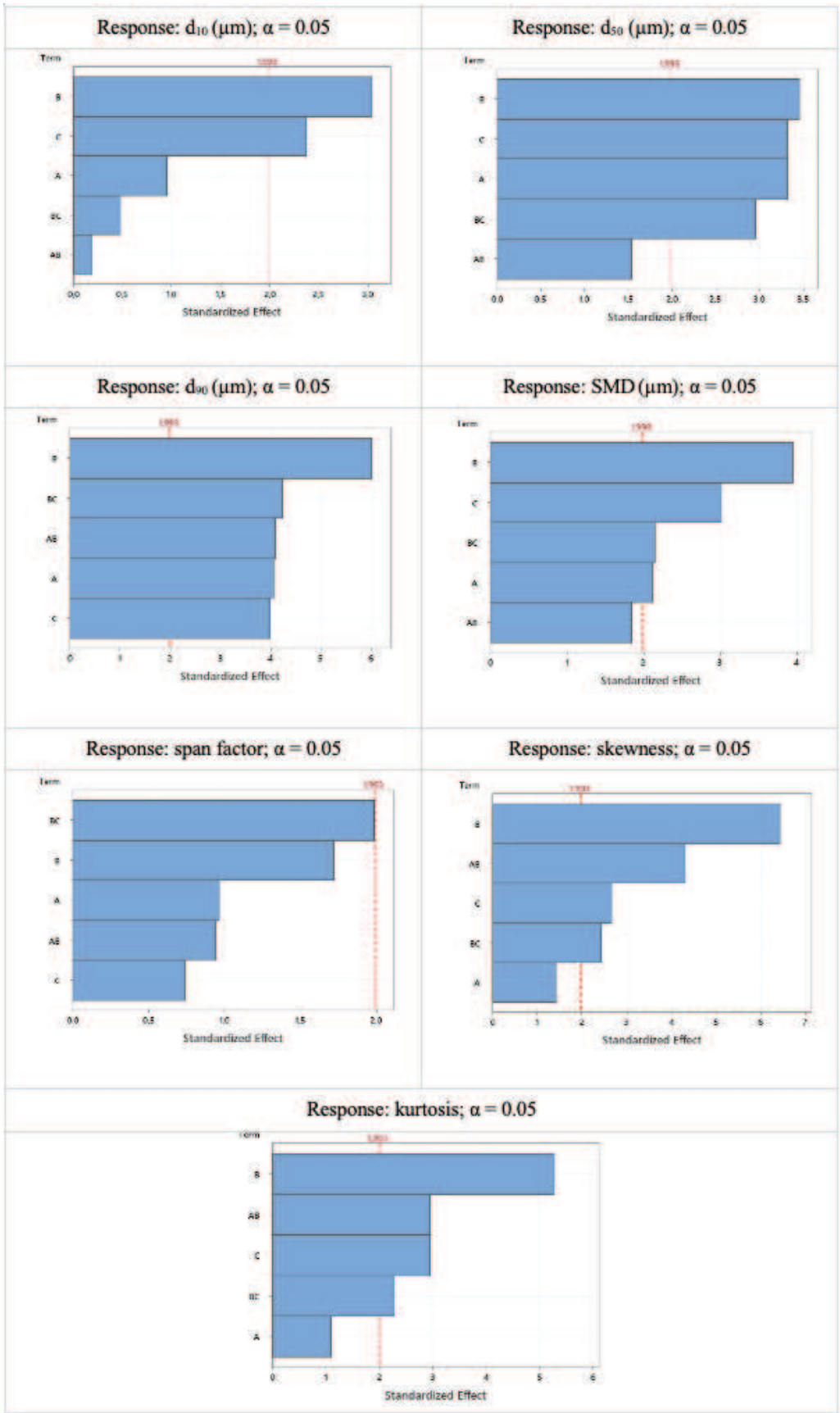


Figure 9: Pareto Charts of the Standardized Effects for d10, d50, d90, SMD, span factor, skewness, and kurtosis (Factors A = orifice diameter, B = air injection pressure, C = fluid

type) with 1.993 being the critical value above which parameters have a statistical significance, and α being the significance level

By comparing the effects relative to the reference line corresponding to a value of 1.993, the following conclusions can be drawn:

a) Factor A, the orifice diameter: this factor showed a significant effect on both d_{50} and d_{90}; however, its effect on the other parameters is low. The orifice diameter, therefore, mainly affects the skewness of the distribution curve, leading to a negatively skewed distribution and indicating the presence of larger droplets but the persistence of smaller ones.
b) Factor B, the air injection pressure: this factor has the largest influence on the presented diameters as well as on the skewness and kurtosis of the distribution curves. Indeed, injecting with a higher air pressure enhances fragmentation, not only leading to the presence of smaller droplets, but also increasing the turbulence level, which leads to an increased chance of coalescence, droplet-droplet interaction, or rainout.
c) Factor C, the fluid type: although its influence is lower than that of factor B, this factor affects all the chosen responses.
d) The span factor is neither significantly affected by the three chosen factors, nor by the persistence time as shown in Table 2.
e) The d_{50} diameter, which is the most common diameter used to characterize a mist or a dispersion, is the most affected by the three factors.

In addition to the listed conclusions, attention should be paid to the influence of the interactions. From the charts above, interactions, such as those between factors B and C (air injection pressure and fluid type), were shown to have an important influence on d_{50} and d_{90}. Such interactions should be studied in detail since their influence on the concentration and turbulence of the mist cloud is not negligible. Another influencing factor to be considered is the electrodes

that were not present when conducting the series of DSD experiments. Such a type of measurement demonstrates the limitations that could be present when increasing the mist concentration or turbulence. Nevertheless, they show that it is possible to characterize a mist cloud when considering all faced obstacles, but also demonstrate that choosing the input parameters one by one (type of nozzle, pressure, fluid) does not ensure to predict the DSD with accuracy. The proposal of a correlation is, therefore, interesting.

The experimental data permitted the establishment of a correlation linking the SMD with liquid and air properties, as well as with injection conditions, represented by the injection velocity. The SMD was chosen as it represents the volume to surface area ratio of the spray and is the most commonly used mean diameter in fuel droplets combustion systems and other applications requiring heat and mass transfer to liquid droplets [25]. A dimensional analysis was, therefore, performed followed by a multiple linear regression allowing to find the following empirical correlation (equation 8):

$$\frac{SMD}{d_o} = 0.0037\left(\frac{\mu_l}{\mu_g}\right)^{-1.15} La^{-0.58} We^{-0.35}\left(\frac{\rho_l}{\rho_g}\right)^{1.74} \quad (8)$$

$$La = \frac{\rho_l d_o \sigma}{\mu_l^2} \quad (9)$$

$$We = \frac{\rho_g V^2 d_o}{\sigma} \quad (10)$$

where *SMD* is the Sauter mean diameter, d_o is the orifice diameter, μ_l and μ_g the liquid and air dynamic viscosities respectively, *La* the Laplace number, *We* the Weber number, ρ_l and ρ_g the liquid and air densities respectively, σ is the liquid surface tension, and *V* is the initial velocity of the exiting jet.

Existing empirical correlations expressing a mean droplet diameter for air-assist external mixing nozzles are numerous. One similar correlation is that established by Elkotb et al. [29] expressed as follows:

$$SMD = 51 d_o Re^{-0.39} We^{-0.18} \left(\frac{\dot{m}_l}{\dot{m}_g}\right)^{0.29} \quad (11)$$

where Re is the Reynolds number and $\dot{m}_l$ and $\dot{m}_g$ are the liquid and air mass flowrates respectively.

It should be noted that the Reynolds number which denotes the ratio of the liquid inertial to the viscous forces (as seen in equation 12) can be replaced by equation 13. The negative effect of both the Laplace and the Weber numbers, seen in both correlations, hence demonstrates the consistency with previous findings.

$$Re = \frac{\rho_l V d_o}{\mu_l} \quad (12)$$

$$Re = \left(We.La.\frac{\rho_l}{\rho_g}\right)^{0.5} \quad (13)$$

3.2 Particle Image Velocimetry (PIV)

The turbulence level of the mist cloud, during and after generation, was quantified for the three nozzle sets and different fluids. Measurements were carried out at an injection pressure of 3 bar for 1-second generations to maintain the precision and visibility of the illuminated droplets. Results showed that the type of fluid did not have significant effects on the turbulence level, represented by the root-mean-squared velocity, at the end of the mist injection. Moreover, calculations were performed instantaneously after the end of the injection to visualize the turbulence level just before ignition (t_v = 1 ms).

Using the data acquired from PIVlab and equation (7), the root-mean-square velocity was calculated for each image corresponding to a specific time. The evolution of v_{rms} with the injection time is depicted in Figure 10, where values of about 1.1 m/s were reached at the end of the mist generation with nozzle set N1 and P_{inj} = 3 bar (hence the instant at which the ignitors would be actuated). This v_{rms} reached a maximum of 1.5 m/s at t_{inj} = 450 ms. A decrease in v_{rms}

occurs after stopping the mist injection at t = 1000 ms as the level of turbulence decreases in the absence of compressed air injection and droplet-droplet interaction. Here, the sedimentation phenomenon takes the lead. Nevertheless, experimental explosion tests were only performed instantaneously after injection when the mist cloud was still considered turbulent. Velocity magnitudes, ranging from 0.5 to 5.5 m/s, were attained at the end of the injection (Figure 5), but higher values were reached during injection with a vertical velocity vector reaching about 15 m/s.

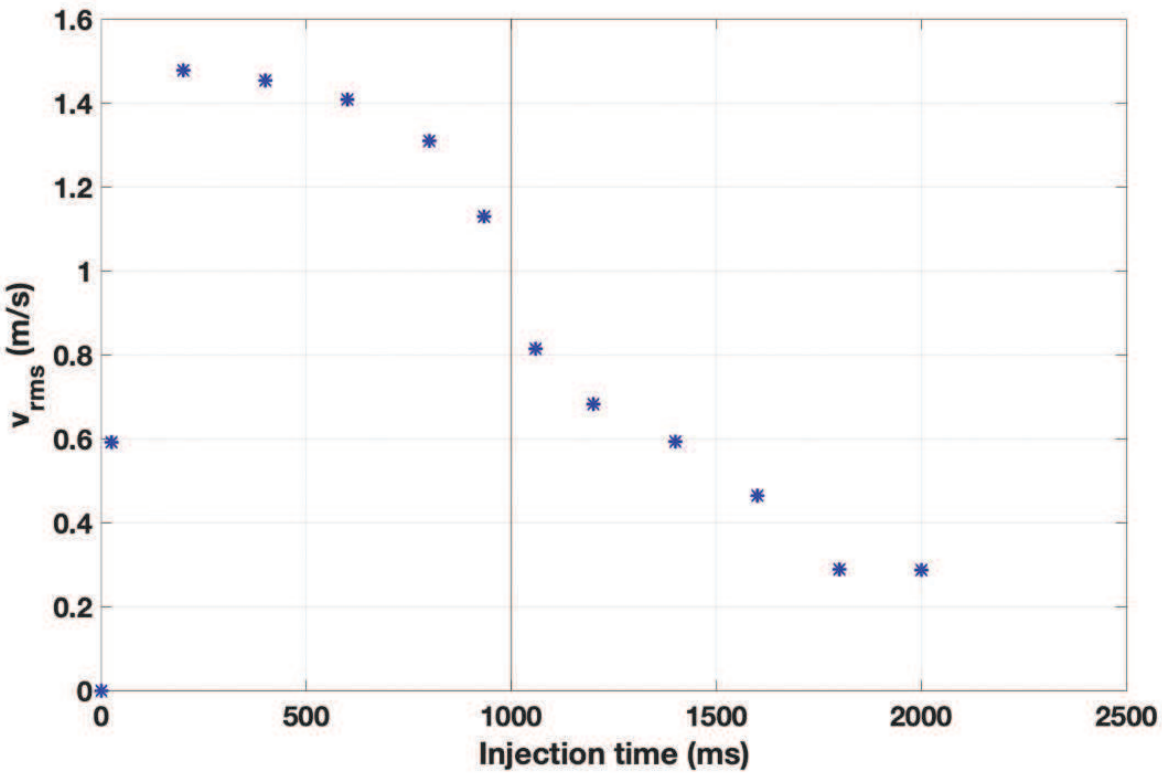


Figure 10: Evolution of the root-mean-square velocity with the mist injection time - generation using nozzle set N1 and P_{inj} = 3 bar

3.3 Ignition sources

Table 3 demonstrates explosion results performed at three different Jet A1 mist concentrations generated by N1 and ignited using both ignition sources (spark ignition and chemical pyrotechnical ignitors). It can be seen that when taking into account the standard errors, both

sources can deliver rather coherent values of both P_m and dP/dt_m when ignited at an energy of 100 J.

Table 3: Comparison between chemical ignitors and spark ignition for Jet A1 mists at three different concentrations

	P_m (bar)			dP/dt_m (bar.s^{-1})		
Mist concentration (g.m^{-3})	**102**	**116**	**130**	**120**	**116**	**130**
Spark ignition (100 J)	5 ± 0.2	5.3 ± 0.2	5.5 ± 0.2	107 ± 28	125 ± 28	158 ± 28
Chemical ignitors (100 J)	4.9 ± 0.2	5.5 ± 0.2	5.1 ± 0.2	80 ± 28	88 ± 28	170 ± 28

3.4 The evaporation model

The d^2-law, developed by Godsave [30], is a simplified droplet evaporation model. It demonstrates that the square of the droplet diameter decreases linearly with time in a diffusion-controlled process. It is generally considered as a well-established law to represent the evaporation of a spherically symmetrical droplet in a fixed environment where the interaction between droplets is considered negligible and the temperature of the droplet is constant and uniform.

Starting with a mass conservation in the gas phase with the hypothesis of a quasi-stationary regime:

$$\dot{m}_v = 4\pi r^2 \rho v = constant \tag{14}$$

The convection-diffusion equations are hence written as follows:

$$\dot{m}_v \frac{dY_v}{dr} = 4\pi r^2 \rho D_v \frac{d^2 Y_v}{dr^2} \tag{15}$$

$$\dot{m}_v C_p \frac{dT}{dr} = 4\pi r^2 \lambda \frac{d^2T}{dr^2} \tag{16}$$

After applying first integration and a mass and energy balance on the droplet's surface, and then solving the evaporation rate equations according to boundary conditions:

$$\dot{m} = \frac{4\pi\lambda_v r_s}{C_{p,}} \ln(B_T + 1) = \ln(1 + B_M) \tag{17}$$

Where B_T and B_M are the thermal and mass transfer Spalding numbers respectively and are equal to the following:

$$B_T = \frac{C_{p,v}(T_\infty - T_d)}{L_v} \tag{18}$$

$$B_M = \frac{Y_{vs} - Y_\infty}{1 - Y_{vs}} \tag{19}$$

Where $C_{p,v}$ is the vapor phase heat capacity, T_∞ and T_d are the temperatures of the surrounding environment and the droplet surface respectively, L_v is the enthalpy of vaporization and Y_{vs} the vapor fraction at stoichiometry and is calculated as follows:

$$Y_{vs} = \frac{x_{vs} M_v}{x_{vs} M_v + (1 - x_{vs}) M_{air}} \tag{20}$$

$$x_{vs} = \frac{P_{sat}(T_s)}{P} \tag{21}$$

$$P_{sat}(T_s) = Ae^{\left(\frac{B}{T_s} - C\right)} \tag{22}$$

A mass balance on the droplet consequently leads to:

$$d^2 = d_0^2 - Kt \tag{23}$$

Where K is the evaporation rate constant of the fuel droplet of initial diameter d_0 and is equal to:

$$K = 8D\frac{\rho}{\rho_l}\ln(1 + B_T) \tag{24}$$

By applying equation (17), a relationship between both the thermal and mass transfer Spalding numbers can be obtained:

$$B_T = (1 + B_M)^{\frac{1}{Le_v}} - 1 \tag{25}$$

where Le is the Lewis number representing the ratio between thermal and mass diffusivities:

$$Le_v = \frac{\lambda}{\rho C_p D} \tag{26}$$

Solving equations 23 to 26 leads to determining the time evolution of the droplet diameter as well as the vapor/liquid ratio at different temperatures in a quiescent environment. Nevertheless, PIV measurements showed that droplet evaporation first takes place in a turbulent environment; therefore, the following equation, considering the mist aerodynamics, can be used in such case [31]:

$$K_t = 8D\frac{\rho}{\rho_l}\ln(1 + B_T)\left(1 + 0.0276Re^{\frac{1}{2}}Sc^{\frac{1}{3}}\right) \tag{27}$$

Where Re is the droplet Reynolds number calculated from PIV data and Sc is the Schmidt number.

The fact that the MIST sphere is a closed vessel should be taken into account. The saturation pressure at a given temperature should hence be considered to define the characteristics of the mist. Moreover, such evaporation can also be studied during the droplet combustion where similar calculations can be carried out in both quiescent and turbulent environments by including the combustion enthalpy Q, the oxygen mass fraction $Y_{Ox,\infty}$, and the mass stoichiometric coefficient s, as follows:

$$B_T = \frac{C_{p,v}(T_\infty - T_d) + \frac{Q}{s}Y_{Ox,\infty}}{L_v} \quad (28)$$

$$B_M = \frac{Y_{Fs} - \frac{Y_{Ox,\infty}}{s}}{1 - Y_{Fs}} \quad (29)$$

Figure 11 shows the influence of the initial ambient temperature on the evaporation time of a Jet A1 droplet of initial diameters of 10 µm, 40 µm, 70 µm, and 100 µm in a turbulent environment with and without combustion. Combustion appears to accelerate the evaporation of the droplet; for example, for a droplet of 10 µm as an initial diameter, the evaporation time at 300 K decreases from about 3 ms to about 0.2 ms in the presence of combustion. It can be seen that as the ambient temperature increases, the contribution of the droplet combustion becomes more negligible. The effect of the ambient temperature is seen to be rather significant on the dynamics of the droplet evaporation; however, starting from about 470 K, a temperature very close to the initial boiling point of Jet A1, this influence begins to decrease. Another pinpointed detail is the influence of the initial droplet diameter, where its increase slows down the droplet evaporation.

However, it should be noted that such models only depict the behavior of a single droplet and do not account for the saturation effect or group interactions caused by nearby vaporizing droplets.

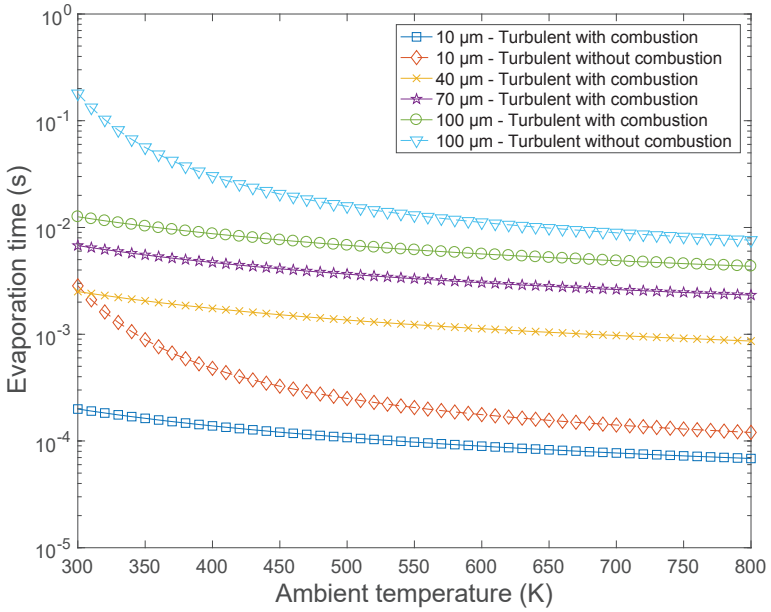


Figure 11: Influence of the ambient temperature and the initial droplet diameter on the evaporation time of a Jet A1 droplet

3.5 Evolution of the mist explosion severity

3.5.1 Influence of the Droplet Size Distribution

The flammability and the explosion severity of a mist are highly influenced by the droplet size distribution. Indeed, Rao and Lefebvre [32] indicated that improving atomization and droplet size distribution is the most effective method to increase the fuel evaporation rate. Bowen and Shirvill [1] also clearly highlighted the critical dependence of the ignition of aerosols on the droplet size for a fixed fuel/air ratio.

Jet A1 mists were generated by the three nozzle sets, N1, N' and N2, at a controlled temperature of 20 °C and varying mist concentrations starting from 80 to 500 g/m^3. Figures 12 and 13 show the evolution of the explosion overpressure and the rate of pressure rise as a function of the fuel mist concentration ignited at 100 J using the chemical ignitors. It can be seen that, at concentrations, both P_m and dP/dt_m tend to decrease with increasing DSD. From a

thermodynamic point of view, the decrease of the maximum explosion pressure can be explained by a lower fuel conversion. Indeed, although ignition takes place in a rather turbulent mist cloud, large droplets may still be affected by gravity resulting in them falling faster than smaller droplets and decreasing the average mist mass concentration at the ignition location. However, other phenomena, such as enhanced drop/wall interaction due to inertial effects of the large droplets should be considered. From a kinetic point of view, the maximum rate of pressure rise is even more sensitive to the DSD: the Sauter mean diameter has a strong influence on the heat transfer, radiative transfers, and evaporation rate (d^2 law of evaporation), which results in a significant decrease of dP/dt_m when the SMD increases.

It should also be noted that high mist concentrations could not be attained by nozzle set N1 since the average concentration tends to change when injecting for a long time. Indeed, the longer the injection, the lower the inter-droplet distance due to higher concentrations. Consequently, not only coalescence is promoted, but also the effects of sedimentation and interaction with the sphere's walls. Moreover, a plateau is reached as the average mist concentration becomes harder to control with high injection durations notably for nozzle sets N' and N2. This endorses the statement of Burgoyne [7], who expressed the difficulty of measuring upper limits of flammability in mist clouds due to the lack of uniformity at high concentrations where an extended range of average concentrations is reached. Table 4 summarizes the values of the maximum explosion overpressure and the maximum rate of pressure rise attained with every nozzle set. These values were determined by assuming that the maximum value corresponds to that found at the beginning of the plateau-like curve. Similar results were obtained by Zhen et al. [33] who studied the explosion characteristics of RP-3 and RP-5 jet fuel mists. Although the droplet size distribution was unknown, their findings on RP-

3 (a Chinese equivalent of Jet A1) mists demonstrate a maximum explosion pressure of around 6.5 bar for a spray injection pressure of about 3.4 bar.

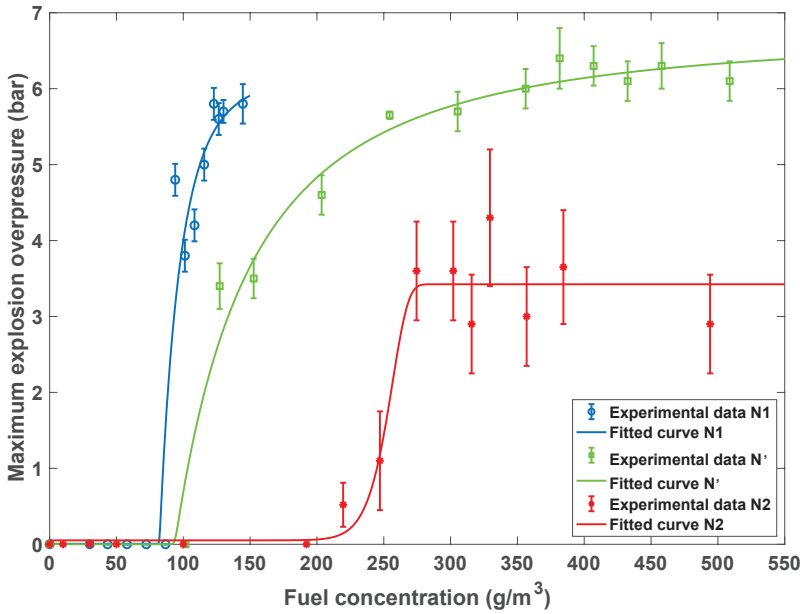


Figure 12: Variation of the maximum explosion overpressure as a function of Jet A1 mist concentrations for nozzle sets N1, N', and N2

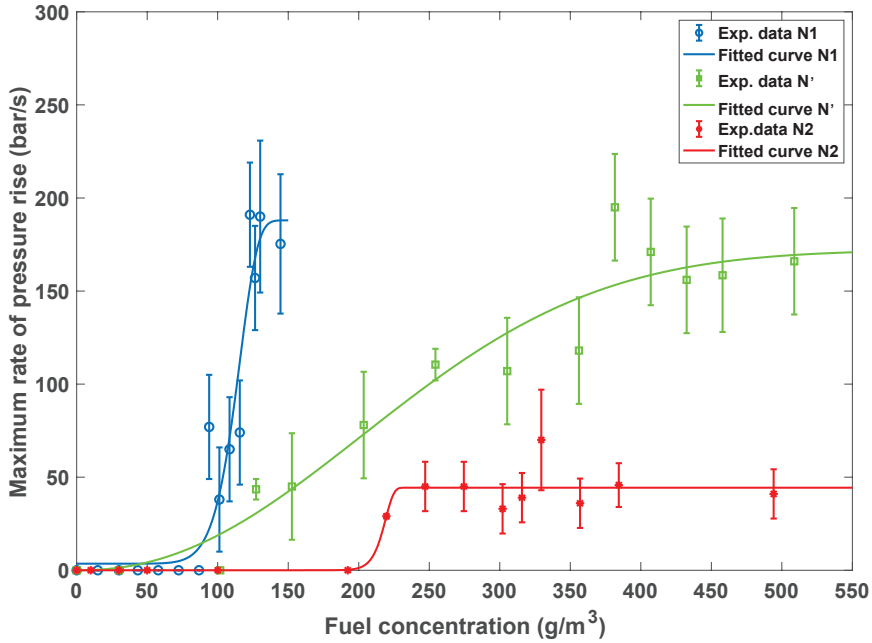


Figure 13: Variation of the maximum rate of pressure rise as a function of Jet A1 mist concentrations for nozzle sets N1, N', and N2

Table 4: Evolution of the explosion severity of Jet A1 mists with the change of DSD

Nozzle set	P_{max} (bar)	dP/dt_{max} (bar/s)	Mist concentration (g/m^3)
N1	5.8	190	125
N'	6.4	195	380
N2	4.3	70	330

3.5.2 Influence of the initial temperature

In a heated atmosphere, the danger of oil leaks cannot be overlooked. Mist may be released in hot crankcase engines, turbines, or heat transfer systems, which can reach temperatures of up to 100 °C. Indeed, in their literature study, Yuan et al. reported an explosion in LaGrange, USA, caused by a heat transfer fluid leak at a high temperature [9]. Moreover, the vapor/liquid ratio is greatly influences by the mist temperature. Therefore, using the water jacket surrounding the MIST sphere, its temperature was set to 27 °C, 40 °C, and 60 °C (± 2 °C) to study the impact of the initial temperature on the mist explosion severity. The liquid was not preheated but temperature measurement performed during the injection of the mist shows that the temperature variation is negligible (2 degrees maximum). Mist mass concentration was varied from about 25 g/m^3 to about 180 g/m^3 with nozzle set N1 at an injection pressure of 3 bar. A spark-ignition source of 100 J was then activated at an initial sphere pressure of 1 bar.

Figures 14 and 15 show that heating the sphere to a temperature greater than the flashpoint of Jet A1 (40°C, Table 1) can indeed alter both explosion overpressures and rates of pressure rise. For instance, the rate of explosion pressure rise increased from values of 145 bar/s at T = 27 °C to about 285 bar/s at T = 40 °C, and then to 540 bar/s at T = 60°C at a mist concentration of 87 g/m^3. The gradual increase of the vapor concentration surrounding the droplet before ignition until reaching the lower explosive limit of Jet A1 vapors explains the changes observed in the figures. Indeed, with the increase of vapor concentration, droplet evaporation does not remain

the only limiting regime of the ignition step which becomes gradually dominated by a gas combustion regime. With the change of the temperature, the maximum explosion pressures were slightly affected as the initial number of moles decreases with increasing temperature. However, results showed that this effect is more noticeable on the rate of pressure rise, hence on the limiting combustion regime and the combustion kinetics of the mist-vapor cloud. It should also be underlined that the effect of the temperature is less perceptible at high mist concentrations, notably starting at a concentration between 115 g/m^3 and 130 g/m^3, where the behavior of both the explosion overpressure and the rate of pressure rise tends to alter at a constant temperature of 60 °C. In fact, when the temperature increases from 20 to 60 °C, the vapor pressure of kerosene rises from 4 to 18 mbar [34]. This suggests that kerosene cannot be entirely vaporized at 60 °C for concentrations more than 125 g/m^3, at which point saturation occurs as demonstrated by using the evaporation model developed in Section 3.4. Furthermore, aside from the early moments of ignition, the flame temperature will swiftly grow above the auto-ignition temperature, with the initial temperature bearing minimal influence. As a result, it appears that at mist concentrations greater than 125 g/m^3, the difference between vapor and mist explosive behavior decreases.

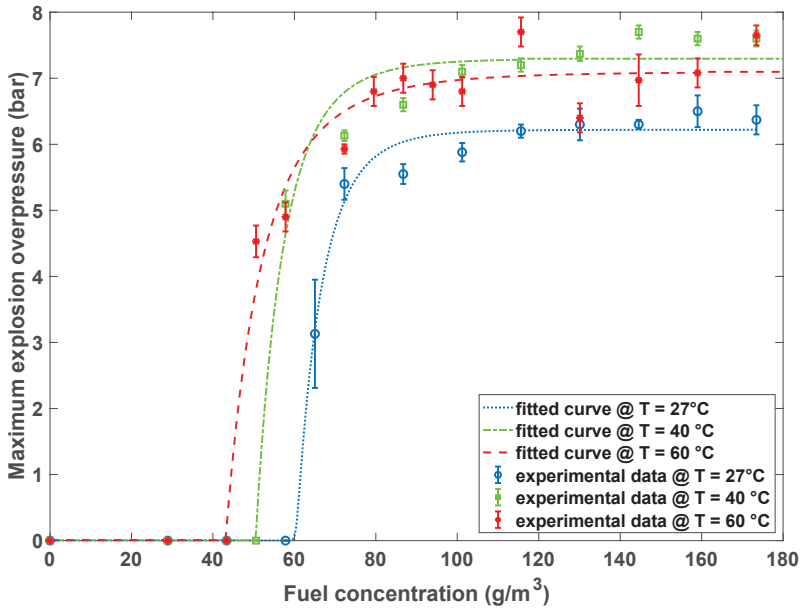


Figure 14: Variation of the maximum explosion overpressure as a function of Jet A1 mist concentration at T = 27, 40 and 60 °C

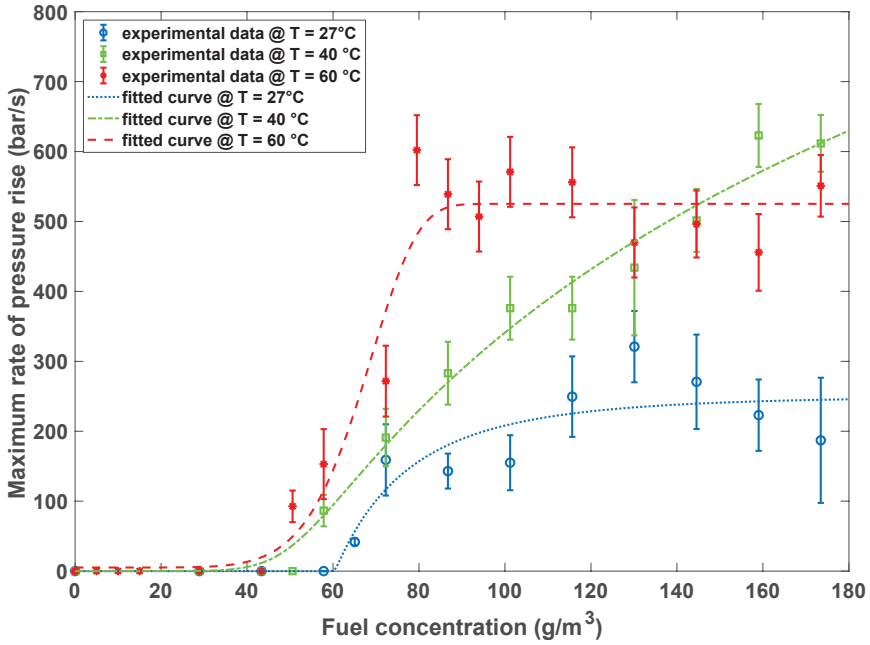


Figure 15: Variation of the maximum rate of pressure rise as a function of Jet A1 mist concentration at T = 27, 40 and 60 °C

Similar tests were carried out using nozzle set N2 providing a d_{50} of about 60 µm. Table 5 shows the values of P_m and dP/dt_m at three different temperatures and mist concentrations of 150, 235, and 455 g/m^3. Mist clouds generated using N2 nozzle exhibited a similar behavior where both thermo-kinetic parameters tended to increase with increasing temperatures.

Table 5: Effect of the sphere temperature on P_m and dP/dt_m for three different Jet A1 mist concentrations generated by nozzle set N2

Mist concentration (g/m^3)	**150**			**235**			**455**		
Temperature (°C)	**27**	**40**	**60**	**27**	**40**	**60**	**27**	**40**	**60**

P_m (bar)	0	5.7	7	1.2	6.6	7.2	4.3	7.4	7
dP/dt_m(bar/s)	0	178	456	47	276	523	67	521	454

As already stated, the vapor concentration in the mist plays a significant role in the rate-limiting step determination. In order to highlight some specificities of Jet A1 mist explosion with regard to gas-phase explosion, theoretical calculations were performed for Jet A using NASA Computer program CEA (Chemical Equilibrium with Applications). Figure 16 shows a slight decrease in the explosion pressure when the temperature increases, which is not the case for the kerosene mists. This trend is probably due to the reduction in the initial number of gas molecules in the closed vessel at a higher temperature, which is confirmed by various studies showing that the explosion pressure of vapors tends to decrease with increasing temperatures while the rate of pressure rise remains rather insensitive to such variations [35–37].

To explain such a difference between theoretical calculations and empirical mist explosion, the evaporation model, detailed in Section 3.4, was utilized by considering the whole mist cloud generated in the MIST sphere. The assumptions were that each mist droplet vaporizes at the same speed and that vaporization begins when the generation stops, which is a strong hypothesis. Moreover, the saturation and the fluctuation of the gas concentration, as a function of temperature, were taken into account. Figures 17(a) and (b) exhibit the evolution of the vapor mass fraction and the normalized vapor ratio (dividing the volume of the generated vapor by 0.6 $\%_{v/v}$, the $LEL_{vapor\text{-}air}$ of Jet A1) as a function of both the initial temperature and droplet diameter. It can be seen from Figure 17(b) that, at T = 40 °C (313 K), the vapor content does not even exceed half the $LEL_{vapor\text{-}air}$. Therefore, kerosene mist would not be completely vaporized, and the DSD would have shifted to lower diameters from that at 27 °C. After 1 ms, ignition would then occur in a two-phase system: small droplets in presence of ‘a layer’ of

kerosene vapor. Such effect, which is usually insignificant, becomes rather considerable when explosions take place at temperatures higher than 20 °C.

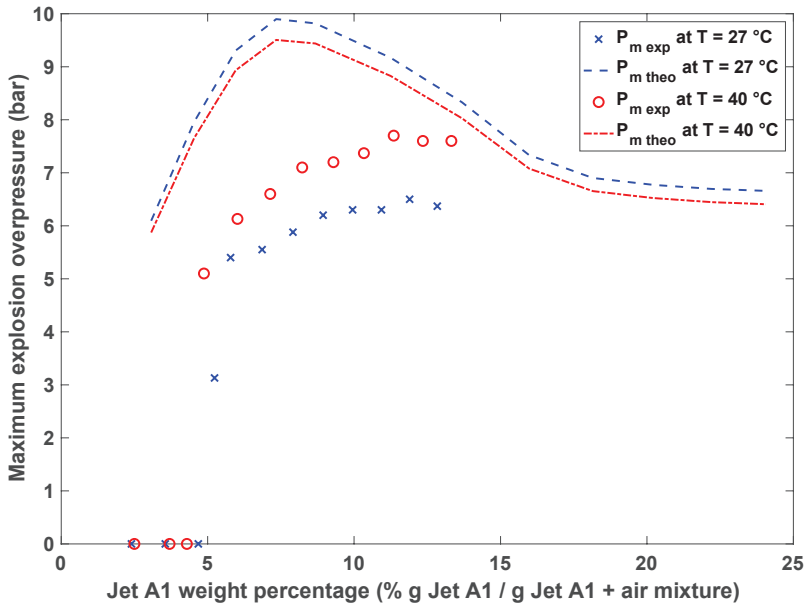


Figure 16: Comparison of theoretical adiabatic explosion overpressure and experimental results for Jet A1 mists at T = 27 and 40 °C

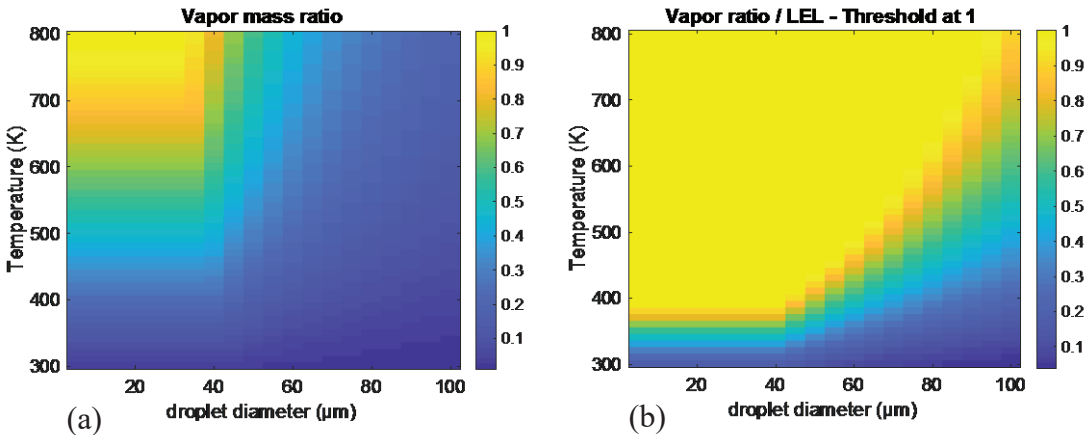


Figure 17: (a) the vapor mass ratio (b) the vapor/LEL ratio as a function of the initial temperature and droplet size for a 4 g Jet A1 mist cloud with a 1 ms delay

Experiments performed at 27 °C were also proceeded by the composition analysis of exhaust gases by micro-gas chromatography (SRA 3000 µGC Analyzer equipped with a thermal conductivity detector). Results showed the continuous but decreasing presence of O_2 accompanied by the appearance of CO as of a mist concentration of 151 g/m^3 (corresponding to about 3 g of injected Jet A1). This quantity of Jet A1, if all droplets were assumed to evaporate and if calculations were carried out on n-dodecane as a suitable Jet A1 surrogate, corresponds to a global theoretical fuel equivalence ratio (Φ) of about 2 (%fuel $_{w/w} \approx 11$). On the other hand, comparing the molar fractions x of the exhaust gases ($x_{CO} = 10^{-3}, x_{CO2} = 0.1,$ and $x_{O2} = 0.05$) to those found by CEA for a wide range of Jet A1 concentrations showed that the molar fractions correspond to a fuel-air mixture of a global experimental Φ of about 0.75. Such finding validates that the injected mist concentration does not correspond to the actual quantity in suspension due to rainout and sedimentation phenomena which also explains the presence of a plateau in explosion pressure-time evolution curves. Nevertheless, it can be seen that µGC tests of explosion exhaust gases, coupled with CEA simulations, could provide a good estimation of the actual mist concentration inside the explosion vessel.

3.6 Mist explosion sensitivity

3.6.1 Minimum Ignition Energy

One of the most important parameters necessary for the assessment of explosion risks and hazardous areas is the minimum ignition energy (MIE). This energy can be defined as the lowest spark energy required to ignite the most easily ignitable mixture of a flammable substance in the air. Nevertheless, it should be noted that this energy is easily influenced by the droplet size distribution, the turbulence of the mist and many other factors. In order to measure this parameter, a high-voltage spark ignition system was developed allowing the control of both the voltage and the spark duration. A Brandenburg 3590-1320 DC/DC converter of 12 V to 10 kV voltage, with a total power of 5 W and a maximum input current of 0.5 mA, was used in this

system. This converter's output may be adjusted, allowing the adjusting of the provided energy to the mist cloud. The real spark duration, as well as the continuous delivered current, would then be calculated to obtain an accurate estimation of the delivered ignition energy. Tests were performed at different mist concentrations using the MIST sphere equipped with the N1 nozzle set at an initial temperature of 27 °C. Figure 18 depicts the variation of the MIE of Jet A1 mist with average concentrations ranging between 110 and 160 g/m^3. This variation exhibits a nearly parabolic behavior, as the fuel concentration shifts from lean to rich, with a minimum of about 200 mJ.

It is common for hydrocarbon fuels to exhibit a lowest ignition energy on the fuel-rich side of the stoichiometric fuel-air ratio. Indeed, Lewis and Von Elbe linked this phenomenon to rapid fuel depletion near the ignition point and the comparatively slow fuel diffusion into this region [38]. As a result, a fuel-rich environment is required to maintain the spark-generated flame kernel developing during the first ignition phase to keep providing fuel molecules to the flame kernel. Therefore, as discussed by Lee et al., an optimum equivalence ratio is maintained within the flame kernel [39]. Nevertheless, it is noteworthy that, because of the multi-component nature of Jet A1 fuels, determining the equivalence ratio under specific conditions is difficult. In reality, for over 300 hydrocarbon species in such a fuel, a precise initial liquid phase composition and all of the Antoine coefficients must be determined. Basing the calculation of the fuel equivalence ratio on n-dodecane, a well-known surrogate of Jet A1, and supposing that all the mist evaporated once ignition occurs, a mist concentration ranging between 130 and 140 g/m^3 can be represented by a theoretical equivalence ratio between 1.5 and 1.75. A local and a global fuel equivalence ratio should be distinguished here. Indeed, the ignition source is actuated instantaneously after the end of the mist injection. Hence, the mist concentration surrounding the ignition source could be considered higher than that near the sphere walls. The minimum ignition energy over the range of tested concentrations is indeed on the fuel-rich side

if we consider a local fuel equivalence ratio in the vicinity of the ignition source. On the other hand, with increasing concentrations, it becomes harder for the flame kernel to be sustained. It is noteworthy that a CFD study is under development to better determine the local mist concentration near the ignition source.

There exist few MIE tests performed on Jet A1 or kerosene mists. Ballal and Lefebvre [40,41] notably tested the ignition sensitivity and flame quenching of such fuel-air mixtures in quiescent conditions and developed a general model for both quiescent and turbulent mist clouds. Their findings demonstrated an MIE, starting from about 800 mJ and descending to about 10 mJ, with an increasing Φ reaching unity in a quiescent mist cloud. Their studies on other hydrocarbons exhibited minimum ignition energies of an order of magnitude between 100 and 300 mJ for diesel and heavy fuel oil mists of an SMD of 60 µm. Studies performed by the US Department of Transportation also showed that the MIE of kerosene-air sprays can reach 15 mJ around 27°C [40,41]. In addition, our results differ from that obtained for gaseous mixtures of Jet A fuel and air, which exhibited MIE as low as 1 mJ at temperatures above 50°C, but were not ignited with 100J at 30°C [40,41].

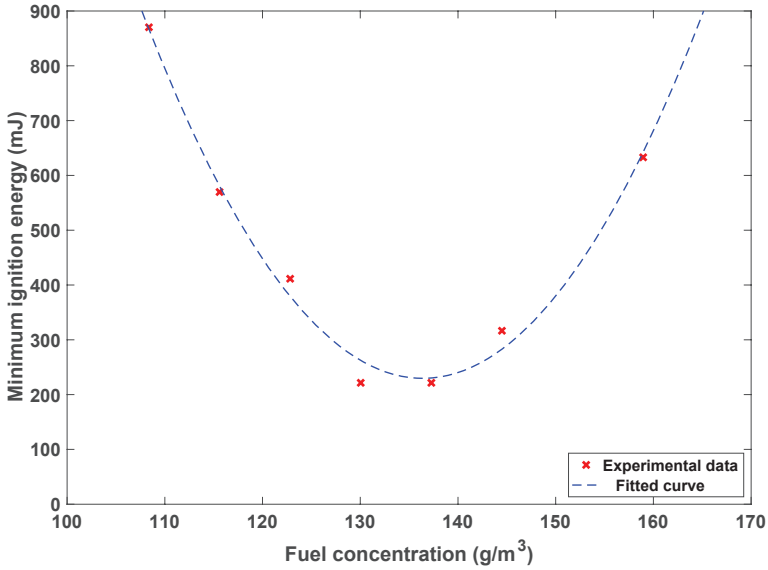


Figure 18: Variation of the minimum ignition energy with Jet A1 mist concentration at T = 27°C

Tests on a higher DSD mist cloud are currently being carried out and show a significant increase of the MIE, corresponding to lower ignition sensitivities.

3.6.2 Lower Explosive Limit

The Lower Explosive Limit (LEL), also known as the Lower Flammability Limit (LFL), is defined as the lowest concentration at which a mixture's flame propagates away from the ignition source. In this study, values of LEL of Jet A1 mists were determined depending on whether an overpressure took place or not. Tables 6 and 7 show how the LEL depends greatly on the DSD and the initial sphere temperature. Its values tend to increase with increasing DSD, a finding rather coherent with that of Zabetakis [42] but incoherent with that obtained by Burgoyne [7]. The author demonstrated that in upward flame propagation tests, LEL values tend to decline as drop diameter increases due to the flame stretching induced by the falling droplets. Nevertheless, such an effect becomes harder to identify when dealing with a spherical or quasi-spherical flame growth as in the 20L sphere.

Table 9 shows that LEL values decrease with increasing temperatures which is logical as it is well known that lower flammability limits tend to decrease while upper limits increase as the temperature is increased [43]. It can be seen from Tables 6 and 7, that at room temperature, LEL values can range between 94 g/m^3 ($1.2\%_{v/v}$) at 20 °C and 65 g/m^3 ($0.8\%_{v/v}$) at 27 °C. It should be noted that in order to present the LEL in percentage vapor, it was assumed that mists fully evaporated at the instant of ignition, which is not the case, as shown in Figures 17 (a) and (b). Using a pilot flame to ignite the mist cloud, Burgoyne stated that the LEL of hydrocarbon mists is roughly 50 g/m^3, especially for tetralin [7]. The author used a pilot flame to ignite the mist cloud. On the contrary, Eckhoff established that values of LEL for a spray range between 100 g/m^3 and 500 g/m^3 regardless of the fuel volatility [2]. Similarly, Dufaud et al. [44] found comparable values of 250 g/m^3 for lube oil mists. For kerosene vapors, Coward and Jones [45] stated that their lower flammability limit, determined in an upward flame propagation tube and

at a temperature sufficient to vaporize kerosene, lies around 0.7%$_{v/v}$. This value is coherent with those obtained in the MIST sphere at elevated temperatures. It is also important to stress that the lower flammability limit of kerosene vapor can be significantly decreased by the presence of mist generated by fuel vibrating or sloshing, for instance [44]. Finally, although consistent with literature data obtained for kerosene or other hydrocarbon fuels, the LEL values are still very dependent on the placement of the ignition source used as well as on the apparatus in which the ignition takes place.

Table 6: LEL of Jet A1 mists as a function of DSD at T = 20°C

Nozzle set	DSD range (µm)	SMD (µm)	D_{10} (µm)	D_{50} (µm)	LEL (g/m^3)	LEL (%$_{v/v}$)
N1	8-10	7	9.2	9	94	1.2
N'	40-60	10	15	14.5	127	1.6
N2	80-100	16.7	7.6	60.5	220	2.8

Table 7: LEL of Jet A1 mists as a function of initial temperature using nozzle set N1

Initial temperature (°C)	LEL (g/m^3)	LEL (%$_{v/v}$)
20	94	1.2
27	65	0.8
40	58	0.7
60	51	0.6

3.6.3. Limiting Oxygen Concentration

The European standard EN 14034-4 [46] for dust clouds defines the Limiting Oxygen concentration (LOC) as the maximum oxygen concentration at which dust explosions no longer occur during three consecutive tests for any given dust concentration. This parameter is usually measured under worst-case-scenario conditions, i.e., when the mixture is most flammable and is usually expressed in percentage of oxygen [47]. It is used as an explosion prevention measure

to inert (decrease the oxygen content in) explosive atmospheres. Mist explosions may be efficiently avoided by maintaining the oxygen concentration below this threshold throughout the whole process system. Studies of LOCs associated with mists are recently scarce and are still limited to some conducted in the twentieth century [7,40,48]. This parameter is dependent on the initial temperature, the type of flammable mixture, and the used inert gas.

For this study, the LOC is considered as the concentration of oxygen below which no flame propagation occurs. To maintain a worst-case scenario, Jet A1 mists were injected into the explosion sphere using the nozzle set N1 at 27 °C. 100 J chemical ignitors were used to ignite the cloud. Nitrogen was used as the inert gas and was injected into the sphere before the mist thereby reducing the oxygen percentage inside the sphere. The LOC was determined using Go/No-Go ignition at least three times per oxygen and mist concentration. Findings showed that Jet A1 mists generated with nozzle set N1 have an LOC of 15.8 $\%_{v/v}$ corresponding to a mist concentration of 144 g/m^{-3}. It can, therefore, be concluded that this mist concentration corresponds to an optimum mist concentration. Such a result can be considered complementary to the previously performed experiments which exhibited plateau-like behaviors.

Table 8: Variation of the minimum oxygen concentration with Jet A1 mist concentration

Mist concentration (g/m^3)	**Oxygen concentration ($\%_{v/v}$)**
116	18.5
130	16.6
144	15.8
160	16.5
174	17

4 Conclusion and perspectives

For the first time, an experimental set-up used to determine both the ignition sensitivity (MIE, LEL and LOC) and explosion severity (P_{max} and dP/dt_{max}) characteristics of mists has been designed and validated. The device is versatile and can test mists of different concentrations, DSD, turbulence, and nature. It is expected to be used in future efforts to standardize testing for the assessment of explosive characteristics of hydrocarbon mists. In this study, this set-up, and the related experimental protocol, were applied to Jet A1 mists, and the influence of the DSD and the initial temperature on the explosion thermo-kinetic parameters was determined.

The following conclusions were drawn:

1. Using the Venturi-based generation system, which was employed for this study, three ranges of droplet diameters can be obtained (from 5 to 120 µm). The DSD of the mist cloud (represented by d_{10}, d_{50}, d_{90}, and SMD diameters) can be significantly influenced by the nozzle orifice diameter, the air injection pressure, and the fluid characteristics. The air injection pressure appears to be the factor with the highest effect. Interactions should be taken into account, for instance through correlations, in order to better characterize the mist cloud.

2. Initial temperatures can significantly alter the explosivity of Jet A1 mists by changing the vapor/liquid ratio of the mist and hence, the rate-limiting step of the combustion. For instance, dP/dt_m increased from values of 145 bar/s at T = 27°C to about 285 bar/s at T = 40 °C, and then to 540 bar/s at T = 60°C at a mist concentration of 87 g/m^3. It can also be observed that even little temperature fluctuations (from 20 °C to 27 °C) can induce changes in experimental values, emphasizing the need to maintain the sphere temperature constant when conducting experiments but also highlighting the impact of such a parameter on industrial mist explosions.

3. Chemical equilibrium calculation (e.g. with CEA NASA), combined and compared with gas chromatography analysis of the composition of the gaseous products, might offer a decent estimation of the actual mist concentration within the explosion vessel, considering droplet-wall interactions, rainout phenomena, and sedimentation.

4. The MIE of Jet A1 for mist concentrations between 110 and 160 g/m^3 demonstrated a parabolic behavior as the concentration increases, reaching a minimum of about 200 mJ at a concentration of about 140 g/m^3 and 27°C. This result is essential for the explosion risks assessment as some studies show that kerosene vapors ignite for energies higher than 100J at this temperature. The potential presence of hydrocarbon mist should therefore be an element that requires reconsidering the classification of hazardous areas.

5. The LEL of Jet A1 mists is highly influenced by the DSD of the mist cloud, as it increases with increasing droplet sizes. Moreover, with increasing initial temperatures, LEL values tend to slightly decrease approaching the LEL of kerosene vapors.

6. The LOC of Jet A1 of droplet diameters ranging between 8 and 10 µm is about 15.8 $\%_{v/v}$ corresponding to a mist concentration of 144 g/m^3. This value corresponds to the optimum mist concentration and complements explosion severity tests.

Although additional tests are required on other hydrocarbon fuels, characterizing the ignition sensitivity and the explosion severity of mists using a single setup was proven possible in this study. The MIST sphere can be considered as a suitable apparatus, simple to find in most of the laboratories and able to give quantitative indications on prevention and protection strategies for hydrocarbon mist explosions.

Acknowledgments

The French Ministry of Ecological Transition and the French Ministry of Higher Education, Scientific Research and Innovation provided financial assistance for this project. The authors would like to express their gratitude to the Health and Safety Executive (UK) for the constructive discussions on the subject. The work's contents, including any opinions and/or conclusions presented, are solely those of the authors and do not necessarily reflect the policies of the French Ministries.

References

[1] Bowen PJ, Shirvill LC. Pressurised atomisation of high flashpoint liquids - implications for hazardous area classification. IChemE Symposium series no. 134, 1994, p. 15.

[2] Eckhoff RK. Generation, ignition, combustion and explosion of sprays and mists of flammable liquids in air: a literature survey. 1995.

[3] Santon RC. Mist fires and explosions – an incident survey 2009:5.

[4] Lees P, Gant S, Bettis R, Vignes A, Lacome JL, Dufaud O. Review of recent incidents involving flammable mists 2019.

[5] Eichhorn J. Careful! Mist can explode. Petroleum Refiner 1955;34(11):194–6.

[6] Burgoyne JH. Mist and spray explosions. Chemical Engineering Progress 1957;53:121–4.

[7] Burgoyne JH. The flammability of mists and sprays. Proc 2nd Symp on Chemical Process Hazards 1963:1–5.

[8] Naegeli DW, Weatherford WD. Basic Research on Mist Flammability. 1977.

[9] Yuan S, Ji C, Han H, Sun Y, Mashuga CV. A review of aerosol flammability and explosion related incidents, standards, studies, and risk analysis. Process Safety and Environmental Protection 2021;146:499–514. https://doi.org/10.1016/j.psep.2020.11.032.

[10] Energy Institute. Model code of safe practice: Area classification code for installations handling flammabe fluids 2015.

[11] Directive 2014/34/EU. Directive 2014/34/EU of the European Parliament and of the Council of 26 February 2014 on the harmonisation of the laws of the Member States relating to

equipment and protective systems intended for use in potentially explosive atmospheres (recast) Text with EEA relevance. vol. OJ L. 2014.

[12] Maragkos A, Bowen PJ. Combustion hazards due to impingement of pressurized releases of high-flashpoint liquid fuels. Proceedings of the Combustion Institute 2002;29:305–11. https://doi.org/10.1016/S1540-7489(02)80041-4.

[13] Willauer HD, Ananth R, Hoover JB, Mushrush G, Williams FW. Chemical Methods for Decreasing Jet Fuel Flammability 2005.

[14] Burrell G, Gant S. Liquid classification for flammable mists 2017.

[15] Dagaut P, Cathonnet M. The ignition, oxidation, and combustion of kerosene: A review of experimental and kinetic modeling. Progress in Energy and Combustion Science 2006;32:48–92. https://doi.org/10.1016/j.pecs.2005.10.003.

[16] Gant S. Generation of flammable mists from high flashpoint fluids: literature review. Health and Safety Executive, Research Report RR980 2013.

[17] Lin Y-R, Chen H, Mashuga C, Mannan MS. Improved electrospray design for aerosol generation and flame propagation analysis. Journal of Loss Prevention in the Process Industries 2015;38:148–55. https://doi.org/10.1016/j.jlp.2015.09.011.

[18] El – Zahlanieh S, Sivabalan S, Dos Santos IS, Tribouilloy B, Brunello D, Vignes A, et al. A step toward lifting the fog off mist explosions: Comparative study of three fuels. Journal of Loss Prevention in the Process Industries 2022;74:104656. https://doi.org/10.1016/j.jlp.2021.104656.

[19] Bowen PJ, Cameron LRJ. Hydrocarbon Aerosol Explosion Hazards: A Review. Process Safety and Environmental Protection 1999;77:22–30. https://doi.org/10.1205/095758299529749.

[20] Lemkowitz SM, Pasman HJ. A Review of the Fire and Explosion Hazards of Particulates. KONA Powder and Particle Journal 2014;31:53–81. https://doi.org/10.14356/kona.2014010.

[21] Santandrea A, Gavard M, Pacault S, Vignes A, Perrin L, Dufaud O. 'Knock on nanocellulose': Approaching the laminar burning velocity of powder-air flames. Process Safety and Environmental Protection 2020;134:247–59. https://doi.org/10.1016/j.psep.2019.12.018.

[22] Kooij S, Sijs R, Denn MM, Villermaux E, Bonn D. What Determines the Drop Size in Sprays? Phys Rev X 2018;8:031019. https://doi.org/10.1103/PhysRevX.8.031019.

[23] Schick RJ. Spray Technology Reference Guide: Understanding Drop Size. Bulletin 459C, Spraying Systems Co.; 2008.

[24] Tascón A. Influence of particle size distribution skewness on dust explosibility. Powder Technology 2018;338:438–45. https://doi.org/10.1016/j.powtec.2018.07.044.

[25] Lefebvre AH, McDonell VG. Atomization and sprays. Second edition. Boca Raton: CRC Press, Taylor & Francis Group, CRC Press is an imprint of the Taylor & Francis Group, an informa business; 2017.

[26] Thielicke W. PIVlab - particle image velocimetry (PIV) tool with GUI. GitHub 2021. https://github.com/Shrediquette/PIVlab/releases/tag/2.53 (accessed July 1, 2021).

[27] EN 15967. Determination of maximum explosion pressure and the maximum rate of pressure rise of gases and vapours. 2022.

[28] Chemical Equilibrium with Applications. Glenn Research Center | NASA 2020. https://www1.grc.nasa.gov/research-and-engineering/ceaweb/ (accessed December 21, 2020).

[29] Elkotb MM, Mahdy M, Montaser ME. Investigation of External-Mixing Air-blast Atomizers. Proceedings of the 2nd International Conference on Liquid Atomization and Sprays, Madison, Wisconsin: 1982, p. 107–15.

[30] Godsave GAE. Studies of the combustion of drops in a fuel spray—the burning of single drops of fuel. Symposium (International) on Combustion 1953;4:818–30. https://doi.org/10.1016/S0082-0784(53)80107-4.

[31] Gökalp I, Chauveau C, Simon O, Chesneau X. Mass transfer from liquid fuel droplets in turbulent flow. Combustion and Flame 1992;89:286–98. https://doi.org/10.1016/0010-2180(92)90016-I.

[32] Rao KVL, Lefebvre AH. Minimum ignition energies in flowing kerosine-air mixtures. Combustion and Flame 1976;27:1–20. https://doi.org/10.1016/0010-2180(76)90002-X.

[33] Zheng L, Changbo L, Gaojun A, Chunhua X, Youjie Z, Lianling R, et al. Comparative Study on Combustion and Explosion Characteristics of High Flash Point Jet Fuel. Procedia Engineering 2014;84:377–83. https://doi.org/10.1016/j.proeng.2014.10.447.

[34] Shepherd JE, Nuyt CD, Lee JJ. Flash Point and Chemical Composition of Aviation Kerosene (Jet A) 2000:38.

[35] Mitu M, Brandes E. Influence of pressure, temperature and vessel volume on explosion characteristics of ethanol/air mixtures in closed spherical vessels. Fuel 2017;203:460–8. https://doi.org/10.1016/j.fuel.2017.04.124.

[36] Razus D, Brinzea V, Mitu M, Movileanu C, Oancea D. Temperature and pressure influence on maximum rates of pressure rise during explosions of propane–air mixtures in a spherical vessel. Journal of Hazardous Materials 2011;190:891–6. https://doi.org/10.1016/j.jhazmat.2011.04.018.

[37] Li Q, Cheng Y, Huang Z. Comparative assessment of the explosion characteristics of alcohol–air mixtures. Journal of Loss Prevention in the Process Industries 2015;37:91–100. https://doi.org/10.1016/j.jlp.2015.07.003.

[38] Lewis B, von Elbe G. Combustion, Flames, and Explosions of Gases. Academic Press, New York, London; 1961.

[39] Lee T-W, Jain V, Kozola S. Measurements of minimum ignition energy by using laser sparks for hydrocarbon fuels in air: propane, dodecane, and jet-A fuel. Combustion and Flame 2001;125:1320–8. https://doi.org/10.1016/S0010-2180(01)00248-6.

[40] Ballal DR, Lefebvre AH. Ignition and flame quenching of quiescent fuel mists. Proceedings of the Royal Society of London A Mathematical and Physical Sciences 1978;364:277–94. https://doi.org/10.1098/rspa.1978.0201.

[41] Ballal DR, Lefebvre AH. A general model of spark ignition for gaseous and liquid fuel-air mixtures. Symposium (International) on Combustion 1981;18:1737–46. https://doi.org/10.1016/S0082-0784(81)80178-6.

[42] Zabetakis MG. Flammability characteristics of combustible gases and vapors. Bureau of Mines, Pittsburgh, PA (United States); 1964. https://doi.org/10.2172/7328370.

[43] Kuchta J. Review of Ignition and Flammability Properties of Lubricants. U.S. Bureau of Mines; 1968.

[44] Dufaud O, Charvet A, Mougel G, Luthun S, Molière M, Brunello D, et al. Generation, Characterization and Ignition of Lube Oil Mists. Volume 4B: Combustion, Fuels and Emissions, Montreal, Quebec, Canada: American Society of Mechanical Engineers; 2015. https://doi.org/10.1115/GT2015-43524.

[45] Coward H, Jones G. Limits of Flammability of Gases and Vapors. Undefined 1952.

[46] EN 14034-4. Determination of explosion characteristics of dust clouds - Part 4: Determination of the limiting oxygen concentration LOC of dust clouds. 2011.

[47] Addai EK, Clouthier M, Amyotte P, Safdar M, Krause U. Experimental investigation of limiting oxygen concentration of hybrid mixtures. Journal of Loss Prevention in the Process Industries 2019;57:120–30. https://doi.org/10.1016/j.jlp.2018.11.016.

[48] Sullivan MV, Wolfe JK, Zisman WA. Flammability of the Higher Boiling Liquids and Their Mists. Ind Eng Chem 1947;39:1607–14. https://doi.org/10.1021/ie50456a021.